Neuropeptidergic circuit modulation of developmental sleep in *Drosophila*

Chikayo Hemmi[1], Kenichi Ishii[1, #], Mana Motoyoshi[1], Masato Tsuji[1] and Kazuo Emoto[1, 2, #, $]

[1]Department of Biological Sciences, Graduate School of Science, The University of Tokyo, 7-3-1 Hongo, Bunkyo-ku, Tokyo 113-0033 Japan

[2]International Research Center for Neurointelligence (WPI-IRCN), The University of Tokyo, 7-3-1 Hongo, Bunkyo-ku, Tokyo 113-0033 Japan

[#]Correspondence: emoto@bs.s.u-tokyo.ac.jp (lead contact), ishii-k@g.ecc.u-tokyo.ac.jp

[$]Lead contact

Abstract

Sleep-wakefulness regulation dynamically evolves along development in flies, fish, and humans. While the mechanisms regulating sleep in adults are relatively well understood, little is known about their counterparts in early developmental stages. Here, we report a neuropeptidergic circuitry that modulates sleep in developing *Drosophila* larvae. Through an unbiased screen, we identified the neuropeptide Hugin and its receptor PK2-R1 as critical regulators of larval sleep. Our data suggest that HugPC neurons secrete Hugin peptides to activate insulin-producing cells (IPCs), which express a Hugin receptor PK2-R1. IPCs, in turn, release *Drosophila* insulin-like peptides (Dilps) to regulate sleep. We further show that the Hugin/PK2-R1 axis is dispensable for adult sleep control. Our findings thus reveal the neuromodulatory circuitry regulating larval sleep, highlighting differential impacts of the same modulatory axis on developmental sleep and adult sleep.

Introduction

Sleep is a fundamental state with significant impacts on many aspects of cognition and metabolism (Blumberg et al., 2005; Davis et al., 2004; Sorribes et al., 2013). While sleep remains essential throughout life, its regulation unfolds dynamically over the course of development. For instance, the pace of sleep-wakefulness cycle is relatively fast in infants, but then gradually slows down and stabilizes in adults (Blumberg et al., 2005; Davis et al., 2004; Sorribes et al., 2013). Furthermore, sleep-wake cycle in infants is independent of circadian rhythm, but it gradually comes under the circadian regulation (Davis et al., 2004; Frank et al., 2017; Poe et al., 2023). Such developmental

evolution of sleep-wakefulness cycles appears to be conserved across flies and mammals, including humans (Blumberg et al., 2005; Davis et al., 2004; Poe et al., 2023; Szuperak et al., 2018). In contrast to the deep insight into the molecular and neural mechanisms underlying adult sleep regulation (Barlow & Rihel, 2017; Scammell et al., 2017; Shafer & Keene, 2021), little is known about regulatory mechanisms underlying infant sleep, partially due to a lack of convenient models to study developmental sleep.

Drosophila larvae have recently emerged as a suitable model for studying sleep regulation mechanisms. Recent studies have reported that the second instar larvae show short periods (< 6 seconds) of an "inactive state" during locomotion. Importantly, this "inactive state" is consistent with the general definition of sleep: reduced responsiveness to noxious stimuli, homeostatic responses to sleep deprivation, and rapid reversibility upon stimulation (Szuperak et al., 2018), suggesting that the "inactive state" might correspond to the sleep state. Interestingly, loss-of-function mutations in the clock genes *clock* and *cyc* fail to impact larval sleep, while significantly altering the sleep patterns in adult flies (Dubowy & Sehgal, 2017; Hendricks et al., 2003; Szuperak et al., 2018). Likewise, mutations in the dopamine transporter *DAT* do not influence larval sleep, while reducing sleep amounts in adults (Kume et al., 2005; Szuperak et al., 2018). These observations imply that sleep regulation mechanisms may be, at least in part, distinct between larvae and adults, yet the neural mechanism of larval sleep remains vastly understudied compared to that of adult sleep.

In this study, we performed an unbiased genetic screen in second-instar larvae, and identified the neuropeptide Hugin and its receptor PK2-R1 as a pair critical for larval

68 sleep control. At the circuit level, Hugin-producing HugPC neurons directly stimulate
69 the insulin-producing cells (IPCs) via PK2-R1 to regulate sleep. Surprisingly, we found
70 that regulators of larval sleep are either irrelevant or exert the opposite effects on adult
71 sleep. Overall, our findings uncover the neuropeptidergic circuitry that regulates larval
72 sleep, and highlight the mechanistic differences between larval and adult sleep.
73

74 **Results**

75 **PK2-R1 is required for sleep control in *Drosophila* larvae**

76 To understand the molecular and neural mechanisms of larval sleep, we modified a
77 previously reported system (Churgin et al., 2019; Szuperak et al., 2018) to automatically
78 quantify the sleep amount of second instar larvae (Figure 1—figure supplement 1) (see
79 Materials & Methods for details). Our system automatically annotates larvae in each
80 frame as either "inactive" or "active" states on the basis of pixel changes, with ~90%
81 accuracy compared to manual annotation (Figure 1—figure supplement 1C). We found
82 that bouts of ≥ 12 inactive frames are consistent with the general criteria for sleep:
83 reduced responsiveness to noxious stimuli, homeostatic responses to sleep loss, and
84 rapid reversibility upon stimulation (Raizen et al., 2008; Szuperak et al., 2018) (Figure
85 1—figure supplement 2. Therefore, the present study defines sleep as an inactive state
86 of ≥ 12 consecutive frames (Figure 1—figure supplement 1A).
87

88 Using this system, we next carried out an unbiased screen for genes involved in sleep
89 regulation. To this end, we tested 47 CRISPR knock-out lines of genes encoding
90 enzymes or receptors for neuropeptides and monoamines (Deng et al., 2019). As

91 illustrated in Figure 1—figure supplement 3, 13 out of 47 homozygous null mutants
92 exhibited significant changes in sleep amounts compared to the control group. To
93 further test the functions of these candidate genes, we next took advantage of the
94 CRISPR knock-in drivers in which GAL4 sequence is inserted into each gene locus.
95 With these drivers, we silenced neurons expressing each candidate gene by expressing
96 the inward-rectifying potassium channel Kir2.1 (Baines et al., 2001). Silencing neurons
97 expressing *Oamb* and *PK2-R1* resulted in a significant sleep decrease, phenocopying the
98 knock-out of these genes (Figure 1A, 1B, and Figure 1—figure supplement 4D). *Oamb*
99 encodes the octopamine receptor and has been reported to be involved in larval sleep
100 (Szuperak et al., 2018). The role of *PK2-R1* in larval sleep, on the other hand, has been
101 unknown to date, prompting us to focus on this gene.
102
103 **Insulin-producing cells express PK2-R1 and regulate sleep in developing larvae**
104 Since the *PK2-R1* driver broadly labeled neurons (~1000 cells) throughout the CNS
105 (Figure 1C), we next attempted to identify a subpopulation of these neurons relevant for
106 sleep regulation. Notably, IPCs in the pars intercerebralis (PI), the neurosecretory center
107 of *Drosophila*, have been reported to express *PK2-R1* (Schlegel et al., 2016).
108 Consistently, the *PK2-R1*$^{2A\text{-}LexA}$ knock-in driver labeled all IPCs (Figure 2A and 2B). To
109 assess whether IPCs are involved in larval sleep, we silenced IPCs with Kir2.1
110 expression using the IPC-specific drivers *Dilp3*- and *Dilp5-GAL4* (Figure 2C). We
111 found that silencing of IPCs significantly increased sleep amounts compared to the
112 control, phenocopying *PK2-R1* neuron silencing and *PK2-R1* knock-out (Figure 1A, 1B,
113 and 2C). Consistently, both *Dilp3* and *Dilp5* null mutants exhibited larger sleep amounts
114 compared to the control (Figure 2D). These phenotypes of *Dilp* mutants IPC silencing

115 are unlikely to be attributed to locomotion defects, as the travel distances during wake
116 periods were unaffected (Figure 2—figure supplement 1B and 1C). Collectively, these
117 findings suggest that *PK2-R1* in IPCs regulates larval sleep.
118
119 **Hugin-expressing neurons control larval sleep**
120 Given that PK2-R1 is a receptor for the neuropeptide Hugin (Rosenkilde et al., 2003),
121 we next examined whether Hugin is involved in larval sleep. We found that *Hug* mutant
122 larvae exhibited significantly larger sleep amounts compared to the control (Figure 3A),
123 consistent with the *PK2-R1* knock-out (Figure 1A). When we silenced *Hug*-expressing
124 neurons by driving the expression of Kir2.1 with the *Hug* CRISPR-knock-in driver
125 $Hug^{2A\text{-}GAL4}$ (Deng et al., 2019), it resulted in a significant increase in sleep amounts
126 without detectable changes in locomotion speed (Figure 3B and Figure 3—figure
127 supplement 1B). Conversely, activation of *Hug*-expressing neurons with the red-shifted
128 channel rhodopsin ReaChR (Inagaki et al., 2014) or the heat-sensitive ion channel
129 TrpA1 (Hamada et al., 2008) both caused a significant reduction in sleep amount
130 (Figure 3C and 3D). These data together indicate that *Hug*-expressing neurons are
131 responsible for downregulating larval sleep.
132
133 *Hug*-expressing neurons are comprised of 20 cells in the subesophageal zone (SEZ) of
134 the brain, and are classified into four subpopulations based on their projection patterns
135 (Bader et al., 2007). Of these, one subpopulation called HugPC neurons (Bader et al.,
136 2007) has been reported to form synaptic connections with IPCs (Hückesfeld et al.,
137 2016). We thus suspected that HugPC neurons may be responsible for sleep regulation.
138 In line with this notion, axons of HugPC neurons labeled by a newly generated *HugPC-*

139 *LexA* driver (Figure 3—figure supplement 2) and IPCs labeled by *Dilp3-GAL4* are
140 located in close proximity to each other (Figure 3E). Indeed, silencing of HugPC
141 neurons by Kir2.1 significantly increased larval sleep (Figure 3F), phenocopying those
142 observed in *Hug* and *PK2-R1* mutants. These results hint at the possibility that HugPC
143 neurons activate IPCs via Hugin/PK2-R1 signaling to regulate sleep.
144
145 **Hugin triggers Ca^{2+} elevation and Dilp secretion in larval IPCs via PK2-R1**
146 A previous report showed that IPCs exhibit increased firing rates and intracellular
147 calcium (Ca^{2+}) levels upon stimulation (Kréneisz et al., 2010). This motivated us to test
148 whether Hugin activates IPCs. To this end, we utilized the recently developed calcium
149 indicator CRTC::GFP, which can report Ca^{2+} dynamics in the timescale of several
150 minutes (Bonheur et al., 2023). As glucose reportedly triggers Ca^{2+} dynamics in IPCs in
151 a range of minutes (Oh et al., 2019), we wondered if CRTC::GFP can detect these
152 dynamics as a positive control. To this end, we applied D-glucose to isolated larval
153 brains and found a significant cytosol-to-nuclear translocation of CRTC::GFP in IPCs
154 within ~5 min, confirming that this reporter can indeed detect Ca^{2+} responses in IPCs
155 upon stimulation (Figure 5A and 5B). We then examined whether *Hug* neurons act
156 upstream of *PK2-R1*-expressing IPCs, by measuring Ca^{2+} responses of IPCs while
157 thermogenetically activating *Hug* neurons with TrpA1 (Figure 4A). In both isolated
158 brains (*ex vivo*) and living larvae (*in vivo*), we found that activation of *Hug* neurons
159 significantly increased Ca^{2+} levels in IPCs (Figure 4B and 4C), suggesting that *Hug*
160 neurons act upstream of IPCs (Figure 4D). Next, we tested whether Hug peptides can
161 induce Ca^{2+} responses in IPCs using *ex vivo* preparations. The *Hug* gene encodes a
162 precursor that potentially produces at least two distinct peptides, Hug-γ and PK-2, both

163 of which can bind PK2-R1 to induce Ca^{2+} responses (Rosenkilde et al., 2003). We thus
164 incubated the CRTC::GFP-expressing larval brain with chemically synthesized Hug-γ or
165 PK-2 (Figure 5A). We found that bath application of either Hug-γ or PK-2 induced
166 significant Ca^{2+} responses in IPCs (Figure 5B–D). In agreement with the idea that Hug
167 peptides activate IPCs via *PK2-R1*, knock-out of *PK2-R1* blocked the Hug peptide-
168 evoked Ca^{2+} elevation in IPCs (Figure 5G). Similar results were obtained when we bath-
169 applied the synthetic Neuromedin U (NMU), the mammalian homlog of Hugin (Figure
170 5A, 5C, and 5G), suggesting that the role of Hugin/PK2-R1 signaling may be conserved
171 across species. Furthermore, Dilp3 accumulated in IPCs was significantly reduced after
172 applying Hug peptides, suggesting that Hugin causes IPCs to release Dilp3 (Figure 5E).
173 Collectively, these data suggest that *Hug* neurons activate IPCs via Hugin/PK2-R1
174 signaling to regulate sleep (Figure 5H).
175
176 **Hugin/PK2-R1 axis has distinct impacts on sleep control in larvae and adults**
177 Given the differences between larval versus adult sleep in temporal pattern and
178 circadian influence, we next wondered if the Hugin/PK2-R1/Dilps axis functions in
179 adult sleep as well. As in larvae, *PK2-R1* knock-out adults showed increased sleep
180 amount compared to the control (Figure 6—figure supplement 1B). In contrast, *Hug*
181 knock-out or silencing of HugPC neurons failed to influence adult sleep (Figure 6A and
182 6B). This suggests that, unlike in larvae, Hug is dispensable for adult sleep.
183 Interestingly, the expression patterns of *PK2-R1* and *Hug*, as well as the morphology of
184 HugPC neurons and IPCs, were almost comparable between larvae and adults (Figure
185 6—figure supplement 2). This implies that the differential roles of Hug in larvae versus
186 adults are likely due to physiological differences in HugPC neurons and/or IPCs. We

187 thus examined how Hug peptides evoke Ca^{2+} responses in adult IPCs and found that
188 neither Hug-γ nor PK-2 could induce Ca^{2+} responses in adult IPCs (Figure 6D and 6E),
189 unlike in larvae. Consistently, Hug peptides failed to reduce Dilp3 levels in adult IPCs
190 (Figure 6F). These data indicate that Hug induces Ca^{2+} responses and Dilp secretion in
191 larval IPCs, but not in adult IPCs. Surprisingly, we further found that *Dilp3* or *Dilp5*
192 null mutations reduced sleep amounts in adults (Figure 6C), while in larvae, these
193 mutations in fact increased the sleep amounts. These data unexpectedly reveal how the
194 same set of neuronal circuits and molecular signaling therein can evolve over
195 development in a complex manner.
196

197 **Discussion**

198 In this study, we have identified the neuropeptide Hugin and its receptor PK2-R1 as a
199 ligand/receptor pair critical for sleep regulation in *Drosophila* larvae. We have further
200 shown that larval IPCs express PK2-R1, respond to and release Dilp3 upon Hugin
201 stimulation. Surprisingly, the Hugin/PK2-R1 axis is dispensable for sleep regulation in
202 adults, even though gene expressions as well as the circuit structure appeared to be
203 conserved between larval and adult brains. Furthermore, Dilps appear to modulate sleep
204 in opposite directions in larvae and adults. Our findings thus uncover the
205 neuropeptidergic modulation circuitry that specifically regulates developmental sleep,
206 and suggest divergent usage of the same molecules and circuitry for sleep modulation in
207 larvae and adults.
208

209 **Hugin/PK2-R1/Dilps axis negatively regulates sleep in larvae**

210 The present study shows that the neuropeptide Hugin and its receptor PK2-R1 are
211 required for sleep regulation in the early larval stage. This notion is supported by the
212 following lines of evidence. First, knock-out mutations in *Hug* or *PK2-R1* increased
213 sleep amounts compared to the control (Figure 1A and 3A). Consistently, silencing a
214 subpopulation of *Hug*-expressing neurons, called HugPC neurons, or *PK2-R1* neurons
215 increased sleep amounts (Figure 1B and 3F). Second, thermogenetic activation of *Hug*
216 neurons decreased sleep amounts (Figure 3D). Third, HugPC neurons project their
217 axons to IPCs in the brain that express PK2-R1 receptors (Figure 3E). Fourth, Hug
218 peptides induced Ca^{2+} elevation and promoted Dilp3 release from IPCs in a PK2-R1-
219 dependent manner (Figure 5). Last, *Dilp3* null mutations increased sleep amounts
220 (Figure 2D). Based on these data, we propose a model in which the Hugin/PK2-
221 R1/Dilps axis along the HugPC-IPC circuitry modulates larval sleep (Figure 7).
222
223 Examples of Hugin acting through PK2-R1 are prominent in the context of feeding
224 regulation in larvae and adults (Schoofs et al., 2014). For example, a recent study has
225 suggested that Hugin regulates the timing of pupariation and body wall contraction
226 during pupariation through PK2-R1 in PTTH neurons (Ohhara et al., 2024). In the
227 present study, we showed that HugPC in the larval brain modulates sleep (Figure 3F). A
228 previous electron microscopic analysis suggested that larval HugPC neurons likely form
229 synaptic connections to downstream neurons, including IPCs (Hückesfeld et al., 2021;
230 Schlegel et al., 2016). We here showed that larval sleep control requires PK2-R1, and
231 that thermogenetic activation of *Hug* neurons causes Ca^{2+} responses in PK2-R1-
232 expressing IPCs (Figure 4). Importantly, our *ex vivo* data indicated that Hugin peptide-
233 induced Ca^{2+} response in IPCs was largely abolished by *PK2-R1* mutation (Figure 5),

234 indicating the critical role of the Hugin/PK2-R1 axis for the HugPC-mediated IPC
235 activation. Together, we propose that the HugPC-IPCs circuity mobilizes Hugin/PK2-
236 R1 signaling to selectively modulate larval sleep. Interestingly, our *ex vivo* data
237 indicated that Neuromedin U (NMU), a mammalian ortholog of Hugin, can trigger Ca^{2+}
238 responses in larval IPCs in a PK2-R1-dependent fashion (Figure 5). Given that NMU
239 has been implicated in sleep regulation in fish and mammals (Ahnaou & Drinkenburg,
240 2011; Chiu et al., 2016), an analogous ligand/receptor pair might be involved in sleep
241 modulation in mammals as well.
242
243 **Divergent roles of insulin in regulation of larval sleep and feeding**
244 IPCs in larvae responded to exogenously applied Hug peptides, both by exhibiting
245 elevated Ca^{2+} levels and decreases in intracellular Dilp3 storage (Figure 5C–E). In
246 contrast to Dilp3, however, the amount of Dilp2 accumulated in IPCs did not decrease
247 following Hug peptide application (Figure 5—figure supplement 1B). On the other
248 hand, Dilp2 accumulation in IPCs decreased after glucose treatment (Figure 5—figure
249 supplement 1A) (Oh et al., 2019). These results unexpectedly suggest that larval IPCs
250 form parallel channels inside, one for Hug-Dilp3 and the other for glucose-Dilp2.
251 Mechanistically, Hug acts directly on IPCs via the PK2-R1 receptor. As for glucose, on
252 the other hand, glucose-sensing CN neurons in the brain take up glucose and
253 subsequently secrete another neuropeptide to activate IPCs (Oh et al., 2019). Such
254 parallelism inside IPCs might provide insights into why insect species broadly express
255 multiple insulin-like peptide genes, in some cases even as many as 40 genes in the
256 silkworm *Bombyx mori* (Okamoto, 2021). *Drosophila* genome harbors eight *Dilp* genes
257 (Nässel et al., 2015), of which *Dilp2*, *Dilp3*, and *Dilp5* are considered nutrient-related.

258 Nevertheless, mRNA expression or release patterns of these Dilps are not identical
259 under different nutrient conditions (Géminard et al., 2024; Nässel et al., 2015; Oh et al.,
260 2019; Ikeya et al., 2002). Furthermore, these Dilps exhibit different binding affinities
261 for the insulin receptor (InR), the secreted decoy of InR (SDR), and the ecdysone-
262 inducible gene L2 (Imp-L2) (Okamoto et al., 2013). These reports hint at the differential
263 roles of different insulin-like peptides; however, mechanistic insights remain largely
264 lacking. Our data on larval IPCs forming parallel channels for Hug-Dilp3 and glucose-
265 Dilp2 may provide a point of entry for tackling this mystery.
266

267 **Differential impacts of the same neuropeptidergic modulations on larval and adult**
268 **sleep**

269 Our data show that the Hugin/PK2-R1/Dilps axis likely downregulates sleep amounts in
270 larvae. Despite the significant increase in sleep amount in *Hug* mutant larvae, *Hug*
271 mutant adults showed sleep amounts comparable to wild-type control (Figure 6A),
272 consistent with a previous report that Hugin is dispensable for control of baseline sleep
273 levels (Schwarz et al., 2021). According to our histological analyses, the Hugin/PK2-R1
274 expression patterns, as well as the HugPC-IPCs circuitry, appear to be largely conserved
275 in adults (Figure 3E and Figure 6—figure supplement 2). Unlike larval brains, however,
276 Hug peptides failed to trigger Ca^{2+} responses in adults IPCs (Figure 6E). It is thus
277 possible that Hugin/PK2-R1 signaling along the HugPC-IPCs circuitry is suppressed in
278 adults. IPCs in adults receive multiple positive and negative modulatory inputs through
279 GPCRs including the metabotropic $GABA_B$ receptors (Enell et al., 2010), which
280 suppress IPC activity and Dilp release in adult IPCs (Enell et al., 2010). It is thus

281 plausible that such negative modulatory inputs to IPCs in adults might counteract the
282 Hugin/PK2-R1 axis to suppress Dilp release. In addition, our data suggest that Dilps
283 modulate sleep amount in the opposite directions in larvae and adults (Figure 7).
284 Comparing the expression levels and activities of GPCRs in larval and adult IPCs would
285 be essential to better understand how same modulatory signals over the course of
286 development come to exert differential impacts on sleep. Interestingly, Hugin in adults
287 appears irrelevant for the baseline sleep amount but is required for homeostatic
288 regulation of sleep (Schwarz et al., 2021). Thus, testing whether the Hugin/PK2-R1 axis
289 is involved in the homeostatic regulation of larval sleep, and how this system compares
290 to its adult counterpart, may further provide mechanistic insights into how homeostatic
291 sleep regulation maturates over development.
292
293 In summary, we identified the Hugin/PK2-R1/Dilps signaling along the HugPC/IPCs
294 circuit as the molecular and circuitry basis for larval sleep regulation. Our study begins
295 to fill the knowledge gap in larval sleep regulation, and sheds light on mechanistic
296 differences in sleep regulation between early developmental stages and adults.
297

298 **Materials and Methods**

299 **Key resource table**

Reagent type (species) or resource	Designation	Source or reference	Identifiers	Additional information
Gene (*Drosophila melanogaster*)	*PK2-R1*	NA	FLYB:FBgn0038140	

Gene (*D. melanogaster*)	*Dilp3*	NA	FLYB:FBgn0044050	
Gene (*D. melanogaster*)	*Dilp5*	NA	FLYB:FBgn0044048	
Gene (*D. melanogaster*)	*Hug*	NA	FLYB:FBgn0028374	
Gene (*Homo sapiens*)	*NMU*	NA	HGNC:7859	
Genetic reagent (*D. melanogaster*)	w^{1118}	Other	NA	Provided by Dr. Yi Rao, Peking University.
Genetic reagent (*D. melanogaster*)	*iso31*	Bloomington *Drosophila* Stock Center	BDSC:5905; RRID:BDSC_5905	Isogenized for chr 1;2;3, with w[1118] line.
Genetic reagent (*D. melanogaster*)	$PK2\text{-}R1^{attP}$	Bloomington *Drosophila* Stock Center	BDSC:84563; RRID:BDSC_84563	FlyBase symbol: TI{TI}PK2-R1[attP]
Genetic reagent (*D. melanogaster*)	$PK2\text{-}R1^{2A\text{-}GAL4}$	Bloomington *Drosophila* Stock Center	BDSC:84686; RRID:BDSC_84686	FlyBase symbol: TI{2A-GAL4}PK2-R1[2A-GAL4]
Genetic reagent (*D. melanogaster*)	$PK2\text{-}R1^{2A\text{-}LexA}$	Bloomington *Drosophila* Stock Center	BDSC:84431; RRID:BDSC_84431	FlyBase symbol: TI{2A-lexA::GAD}PK2-R1[2A-lexA]
Genetic reagent (*D. melanogaster*)	$Dilp3^{1}$	Bloomington *Drosophila* Stock Center	BDSC:30882; RRID:BDSC_30882	FlyBase symbol: TI{TI}Ilp3[1]
Genetic reagent (*D. melanogaster*)	$Dilp5^{1}$	Bloomington *Drosophila* Stock Center	BDSC:30884; RRID:BDSC_30884	FlyBase symbol: TI{TI}Ilp5[1]
Genetic reagent (*D. melanogaster*)	*Dilp3-GAL4*	Bloomington *Drosophila* Stock Center	BDSC:52660; RRID:BDSC_52660	FlyBase symbol: P{Ilp3-GAL4.C}2

Genetic reagent (*D. melanogaster*)	*Dilp5-GAL4*	Bloomington *Drosophila* Stock Center	BDSC:66007; RRID:BDSC_66007	FlyBase symbol: P{Ilp5-GAL4.L}8
Genetic reagent (*D. melanogaster*)	Hug^{attP}	Bloomington *Drosophila* Stock Center	BDSC:84514; RRID:BDSC_84514	FlyBase symbol: TI{TI}Hug[attP]
Genetic reagent (*D. melanogaster*)	$Hug^{2A\text{-}GAL4}$	Bloomington *Drosophila* Stock Center	BDSC:84646; RRID:BDSC_84646	FlyBase symbol: TI{2A-GAL4}Hug[2A-GAL4]
Genetic reagent (*D. melanogaster*)	$Hug^{2A\text{-}LexA}$	Bloomington *Drosophila* Stock Center	BDSC:84397; RRID:BDSC_84397	FlyBase symbol: TI{2A-lexA::GAD}Hug[2A-lexA]
Genetic reagent (*D. melanogaster*)	*HugPC-GAL4*	Hückesfeld et al., 2016 (DOI:10.1038/ncomms12796)	NA	Provided by Dr. Michael J. Pankratz, University of Bonn.
Genetic reagent (*D. melanogaster*)	*HugPC-LexA*	This paper	NA	The 544-bp enhancer region of Hug was placed upstream of nlsLexA::p65, and the construst was inserted into attP2 site by ΦC31 integrase-mediated transgenesis. See Methods for details.
Genetic reagent (*D. melanogaster*)	*UAS-Kir2.1::EGFP*	Bloomington *Drosophila* Stock Center	BDSC:6596; RRID:BDSC_6596	FlyBase symbol: P{UAS-

				Hsap¥KCNJ2.EGFP}1
Genetic reagent (*D. melanogaster*)	*UAS-Stinger, LexAop-tdTomato.nls*	Bloomington *Drosophila* Stock Center	BDSC:66680; RRID:BDSC_66680	FlyBase symbol: P{UAS-Stinger}2; PBac{13XLexAop2-IVS-tdTomato.nls}VK00022
Genetic reagent (*D. melanogaster*)	*UAS-mCD8::mCherry, UAS-CRTC::GFP*	Bloomington *Drosophila* Stock Center	BDSC:99657; RRID:BDSC_99657	FlyBase symbol: P{UAS-mCD8.mCherry-T2A-lacZ.nls}JK22C; P{UAS-Crtc.GFP}attP40
Genetic reagent (*D. melanogaster*)	*UAS-ReaChR*	Bloomington *Drosophila* Stock Center	BDSC:53741; RRID:BDSC_53741	FlyBase symbol: P{UAS-ReaChR}attP40
Genetic reagent (*D. melanogaster*)	*UAS-TrpA1*	Bloomington *Drosophila* Stock Center	BDSC:26263; RRID:BDSC_26263	FlyBase symbol: P{UAS-TrpA1(B).K}attP16
Genetic reagent (*D. melanogaster*)	*LexAop-TrpA1*	Burke et al., 2012 (DOI:10.1038/nature11614)	NA	Provided by Dr. Scott Waddel, University of Oxford.
Genetic reagent (*D. melanogaster*)	*LexAop-rCD2::RFP-p10.UAS-mCD8::GFP-p10*	Bloomington *Drosophila* Stock Center	BDSC:67093; RRID:BDSC_67093	FlyBase symbol: P{lexAop-rCD2::RFP-p10.UAS-mCD8::GFP-p10}su(Hw)attP5

Genetic reagent (*Escherichia coli*)	One Shot™ *ccdB* Survival™ 2 T1^{R} competent cells	Thermo Fisher Scientific	Thermo Fisher Scientific:A10460	
Antibody	Anti-GFP (chicken polyclonal)	Aves Labs	Aves Labs:GFP-1020; RRID:AB_10000240	IHC (1:1000)
Antibody	Anti-mCherry (mouse monoclonal)	Takara Bio	Takara Bio:632543; RRID:AB_2307319	IHC (1:1000)
Antibody	Anti-Dilp3 (rabbit polyclonal)	Veenstra et al., 2009 (DOI:10.1007/s00441-009-0769-y)	NA	IHC (1:250) Provided by Dr. Jan A. Veenstra, Université de Bordeaux.
Antibody	Anti-Dilp2 (rabbit polyclonal)	Okamoto et al., 2012 (DOI:10.1073/pnas.1116050109)	NA	IHC (1:2000) Provided by Dr. Takashi Nishimura, RIKEN.
Antibody	Anti-brp (mouse monoclonal)	Developmental Studies Hybridoma Bank	DSHB:nc82; RRID: AB_2314866	IHC (1:100)
Antibody	Anti-histone H3 phospho S28 (rat monoclonal)	Abcam	Abcam:ab10543; RRID:AB_2295065	IHC (1:1000)
Antibody	Goat anti-chicken Alexa Fluor 488	Thermo Fisher Scientific	Thermo Fisher Scientific:A-11039; RRID:AB_2534096	IHC (1:200)

Antibody	Goat anti-mouse Alexa Fluor 555	Thermo Fisher Scientific	Thermo Fisher Scientific:A-21424; RRID:AB_141780	IHC (1:200)
Antibody	Goat anti-rabbit Alexa Fluor 633	Thermo Fisher Scientific	Thermo Fisher Scientific:A-21071; RRID:AB_2535732	IHC (1:200)
Antibody	Goat anti-rat Alexa Fluor 633	Thermo Fisher Scientific	Thermo Fisher Scientific:A-21094; RRID:AB_2535749	IHC (1:200)
Recombinant DNA reagent	pBPnlsLexA::p65Uw	Addgene	Addgene:26230; RRID:Addgene_26230	
Sequence-based reagent	*HugPC* enhancer	This paper	NA	A 544-bp fragment PCR-amplified from the fly genomic DNA. See Methods for details.
Peptide, recombinant protein	Hug-γ	This paper	NA	Chemically synthesized *Drosophila* Hug-γ peptide with amino acid sequences of Acetyl-QLQSNGEPAYRVRTPRL-CONH2

Peptide, recombinant protein	PK-2	This paper	NA	Chemically synthesized *Drosophila* PK-2 peptide with amino acid sequences of Acetyl-SVPFKPRL-CONH2
Peptide, recombinant protein	NMU	This paper	NA	Chemically synthesized human NMU peptide with amino acid sequences of Acetyl-FRVDEEFQSPFASQSRGYFLFRPRN-CONH2
Commercial assay or kit	PrimeSTAR Max DNA Polymerase	Takara Bio	Takara Bio:R045A	
Commercial assay or kit	In-Fusion HD Cloning Kit w/Cloning Enhancer	Takara Bio	Takara Bio:639635	
Chemical compound, drug	D(+)-Glucose	FUJIFILM Wako Pure Chemical Corporation	FUJIFILM Wako Pure Chemical Corporation:041-00595	
Software, algorithm	Adobe Illustrator 2023	Adobe	RRID:SCR_010279	
Software, algorithm	Adobe Photosop 2023	Adobe	RRID:SCR_014199	

Software, algorithm	ImageJ v1.53t	Schneider et al., 2012 (DOI:10.1038/nmeth.2089)	RRID:SCR_003070	
Software, algorithm	Inkscape v1.2	The Inkscape Team	RRID:SCR_014479	
Software, algorithm	Prism v9.5.1	GraphPad	RRID:SCR_002798	
Software, algorithm	Python Programming Language v3.10.0	Python Software Foundation	RRID:SCR_008394	
Software, algorithm	R Project for Statistical Computing v4.1.2	R Core Team 2021	RRID:SCR_001905	
Software, algorithm	SnapGene v5.3.3	GSL Biotech LLC	RRID:SCR_015052	
Software, algorithm	Arduino UNO	Arduino	RRID:SCR_017284	
Software, algorithm	TriKinetics DAMSystem3 Software	TriKinetics Inc. (available at https://trikinetics.com/)	RRID:SCR_021809	
Other	TriKinetics Drosophila Activity Monitoring System	TriKinetics Inc.	RRID:SCR_021798	
Other	Fan-less Peltier-type incubator	Mitsubishi Electric Engineering Co., Ltd.	Mitsubishi Electric Engineering Co., Ltd.:SLC-25	Used to keep flies for DAM experiments.

300

301 **Fly strains**

302 The following strains of *Drosophila melanogaster* were obtained from the Bloomington
303 *Drosophila* Stock Center: *iso31* (an isogenic w^{1118} strain; BDSC# 5905), *PK2-R1*^{attP}
304 (BDSC# 84563), *PK2-R1*$^{2A\text{-}GAL4}$ (BDSC# 84686), *PK2-R1*$^{2A\text{-}LexA}$ (BDSC# 84431),
305 *Dilp3*^{1} (BDSC# 30882), *Dilp5*^{1} (BDSC# 30884), *Dilp3-GAL4* (BDSC# 52660), *Dilp5-*
306 *GAL4* (BDSC# 66007), *Hug*^{attP} (BDSC# 84514), *Hug*$^{2A\text{-}GAL4}$ (BDSC# 84646), *Hug*$^{2A\text{-}LexA}$
307 (BDSC# 84397), *UAS-Kir2.1::EGFP* (BDSC# 6596), *UAS-Stinger, LexAop-*
308 *tdTomato.nls* (BDSC# 66680), *UAS-mCD8::mCherry, UAS-CRTC::GFP* (BDSC#
309 99657), *UAS-ReaChR* (BDSC# 53741), *UAS-TrpA1* (BDSC# 26263), *LexAop-ReaChR*
310 (BDSC# 53746), *LexAop-rCD2::RFP-p10.UAS-mCD8::GFP-p10* (BDSC# 67093).
311 w^{1118} was from Y. Rao (Peking University); *HugPC-GAL4* (Hückesfeld et al., 2016) was
312 from M. Pankratz (University of Bonn); *LexAop-TrpA1* (Burke et al., 2012) was from S.
313 Waddel (University of Oxford). *HugPC-LexA* was generated in this study (see the
314 following section, "Generation of transgenic lines"). Detailed lists of fly genotypes can
315 be found in the key resource table and Source Data files.

316

317 **General fly maintenance**

318 Flies were maintained on conventional fly food under a 9AM:9PM light/ dark cycle at
319 25°C and 60 +/- 5 % humidity.

320

321 **Egg collection**

322 Agar substrates for egg collection were prepared by microwaving a mixture of 2.0 g
323 sucrose (Fujifilm Wako Pure Chemicals, cat# 196-00015), 3.0 g agar (BD, cat#

324 214010), 2.5 mL apple juice (Dole), and Milli-Q water up to 100 mL. Melted agar was
325 poured into Petri dishes with a diameter of 4 cm (approximately 3 mL per dish).
326 Solidified agar was scratched with tweezers to make the surface rough. Agar plates were
327 stored inside a sealed container at 4°C. Upon egg collection, yeast paste (dried yeast
328 (Nippon Beet Sugar Co., Ltd.) kneaded with Milli-Q water at 40% (w/w)) was placed in
329 the center of the agar plates to further promote oviposition.
330
331 **Larval staging**
332 First-instar larvae were collected two days after egg collection. Among them, second-
333 instar larvae that molted within 2 h were used for video recording. The distinction
334 between first- and second-instar larvae was based on morphological characteristics:
335 while anterior spiracles were not evident in the first-instar, fist-shaped spiracles were
336 observed in the second-instar.
337
338 **Larval sleep analysis**
339 Twenty-four-well silicone chambers for sleep analysis, described in Figure 1—figure
340 supplement 1B, were made by pouring dimethylpolysiloxane (PDMS) into molds based
341 on a previous study (Churgin et al., 2019; Szuperak et al., 2018). As a substrate, 120 μL
342 of a mixture of 3% agar and 2% sucrose was poured into each well. After the gel
343 solidified, 10 μL of 60 mg/mL yeast suspension was applied to the surface of the gel in
344 each well. One larva was transferred into each well, and a glass plate (Azone, cat# 1-
345 4540-01, 5 mm × 200 mm × 200 mm) was placed on top of the chamber to prevent the
346 larvae from escaping. The chamber was placed inside a dark box equipped with a ring-
347 type infrared LED (CCS, cat# LDR2-132IR940-LA) and a camera (The Imaging

348 Source, cat# DMK27BUP031), and recording was started immediately without
349 acclimation. Images were captured through the IC Capture software (The Imaging
350 Source, version 2.5) placed above the chamber under the following conditions: MJPEG
351 Compressor for codec, a frame rate of 0.87 fps, and an image size of 2592 × 1944. For
352 each well and frame, the image of larva was blurred and binarized to automatically
353 locate the larva. Consecutive frames were then compared so that changes in values were
354 summed to estimate the larval motion. This motion estimate was then used to classify
355 every consecutive pair of frames as representing "active" or "inactive." We found that
356 inactivity across 12 consecutive frames meets the sleep criteria, as shown in Figure 1—
357 figure supplement 2.
358
359 **Sleep deprivation**
360 Blue light irradiation was performed using a 455-nm LED (Thorlabs, cat# M455L4)
361 with a collimating adapter (Thorlabs, cat# SM1U25-A). The irradiation intensity was set
362 to the maximum scale using a T-cube LED driver (Thorlabs, cat# LEDD1B). Temporal
363 control of the LED illumination was achieved using an Arduino UNO microcontroller
364 board (Arduino, RRID:SCR_017284). For sleep deprivation experiments, the first 1 h
365 was recorded without LED illumination, followed by another 1 h consisting of repeated
366 cycles of "LED ON for 90 s and OFF for 30 s."
367
368 **Immunohistochemistry**
369 The following steps were carried out in succession: dissection in phosphate-buffered
370 saline (PBS); fixation in 4% paraformaldehyde/PBS at room temperature for either 90
371 min in CRTC::GFP experiments or 30 min in the others; washing with 0.3% Triton X-

372 100/PBS (hereafter referred to as PBST) for 10 min × 3; blocking in 5% normal goat
373 serum (NGS)/PBST at room temperature for 30 min; primary antibody treatment at 4°C
374 overnight; washing with PBST for 10 min × 3; secondary antibody treatment at 4°C
375 overnight; washing with PBST for 10 min × 3; and mounting in VECTASHIELD
376 medium (Vector Laboratories, cat# H-1000, RRID:AB_2336789). The above steps were
377 performed either in Terasaki 96-well plates (stem Corp., cat# P96R37N) for adults or in
378 48-well culture plates (Corning, cat# 3548) for larvae. The following primary antibodies
379 were diluted in 5% NGS/PBST: chicken polyclonal anti-GFP (1:1000, Aves Labs, cat#
380 GFP-1020, RRID:AB_10000240), mouse monoclonal anti-mCherry (1:1000, Takara
381 Bio, cat# 632543, RRID:AB_2307319), rabbit polyclonal anti-Dilp3 (1:250, (Veenstra
382 et al., 2008)), rabbit polyclonal anti-Dilp2 (1:2000, (Okamoto et al., 2012)), mouse
383 monoclonal anti-BRP (1:100, Developmental Studies Hybridoma Bank, clone nc82;
384 RRID:AB_2314866), and rat monoclonal anti-histone H3 phospho S28 (1:1000,
385 Abcam, cat# ab10543; RRID:AB_2295065). The following secondary antibodies were
386 diluted in 5% NGS/PBST: goat anti-chicken Alexa Fluor 488 (1:200, Thermo Fisher
387 Scientific, cat# A-11039, RRID:AB_2534096), goat anti-mouse Alexa Fluor 555 (1:200,
388 Thermo Fisher Scientific, cat# A-21424, RRID:AB_141780), goat anti-rabbit Alexa
389 Fluor 633 (1:200, Thermo Fisher Scientific, cat# A-21071, RRID:AB_2535732), and
390 goat anti-rat Alexa Fluor 633 (1:200, Thermo Fisher Scientific, cat# A-21094;
391 RRID:AB_2535749). Fluorescence images were obtained using a confocal microscope
392 (Leica, TCS SP8) with 20× (Leica, HC PL APO CS2 20×/0.75 IMM) and 63× (Leica,
393 HC PL APO CS2 63×/1.40 OIL) objectives. Images were captured at 512 × 512 pixel
394 resolution in 1 μm-steps along the z-axis. Z-stack images of the maximum projections
395 were generated using the ImageJ v1.53t software ((Schneider et al., 2012);

396 RRID:SCR_003070).

397

398 **Generation of transgenic lines**

399 *HugPC-LexA* lines were generated by ΦC31 integrase-mediated transgenesis, as
400 previously described (Groth et al., 2004). The 544-bp enhancer region of *Hug,* identical
401 region to that used for *HugPC-GAL4* (Hückesfeld et al., 2016), was PCR-amplified
402 from fly genomic DNA. The gel-purified amplicon was subjected to another round of
403 PCR to add hangout sequences. The backbone suicide-vector pBPnlsLexA::p65Uw
404 (RRID:Addgene_26230) was initially amplified by transforming the *ccdB*-resistant *E.*
405 *coli* strain, One Shot™ *ccdB* Survival™ 2 $T1^R$ competent cells (Thermo Fisher
406 Scientific, cat# A10460). The PCR product and the vector were digested by Aat II
407 (NEB, cat# R0117S) and Fse I (NEB, cat# R0588S), followed by ligation using In-
408 Fusion HD Cloning Kit w/Cloning Enhancer (Takara Bio, cat# 639635). The integrity of
409 the resulting plasmid was confirmed by DNA sequencing. Plasmid insertion was
410 targeted to four attP sites (attP2, attP40, VK00005, and su(Hw)attP5) individually
411 through ΦC31 integrase-mediated transgenesis by BestGene Inc. (Chino Hills, CA).
412 Transformants were selected based on the eye color marker. Among the generated
413 strains harboring *HugPC-LexA* in each insertion site, labeling patterns in the larval brain
414 were checked by driving fluorescent marker expression under the control of *LexAop*
415 sequence (Figure 3—figure supplement 2). As the *HugPC-LexA* inserted in attP2
416 closely resembled the labeling pattern of the original *HugPC-GAL4*, we chose this
417 driver in further experiments.

418 The following primers were used for cloning:

419 Forward primer for the *HugPC* enhancer; 1st round PCR against genomic DNA:

420 5’-AAGGGTTTGGTTTAATTTATTTATGTCATA-3’

421 Reverse primer for the *HugPC* enhancer; 1st round PCR against the genomic DNA:

422 5’-GGACAACTGATGCCAGCAGC-3’

423 Forward primer for the *HugPC* enhancer with hangout sequences (underlined); 2nd

424 round PCR against the 1st round amplicon:

425 5’-gaaaagtgccacctgacgtAAGGGTTTGGTTTAATTTATTTATGTCATA-3’

426 Reverse primer for the *HugPC* enhancer with hangout sequences (underlined); 2nd round

427 PCR against the 1st round amplicon:

428 5’-cccgggcgagctcggccggGGACAACTGATGCCAGCAGC-3’

429

430 **Measurement of neuronal activity and Dilp3 accumulation in IPCs**

431 The GFP-tagged CRTC (CRTC::GFP) reporter was applied to quantify the activities of

432 larval IPCs, essentially according to the previous report in adult flies (Bonheur et al.,

433 2023). Parental *Dilp3-GAL4* and the reporter line harboring *UAS-CRTC::GFP* and

434 *UAS-mCD8::mCherry* (BDSC# 99657) were crossed, and eggs were collected within an

435 8–10 h time window. Offspring larvae were reared for 4 days after egg laying (AEL) at

436 25°C until the early third instar. Collected larvae were washed with water and starved

437 on water-soaked paper for 12–14 h. For *in vivo* thermogenetic activation, larva-

438 containing Petri dishes were warmed at 30°C for 60 min. For *ex vivo* thermogenetic

439 experiments, larvae were dissected in calcium- and sugar-free HL3.1 buffer (Nakamizo-

440 Dojo et al., 2023) and each brain was incubated in the same buffer at 30°C for 5 min.

441 For *ex vivo* glucose or peptide application assays, larvae were first dissected in the same

442 buffer as above at room temperature, and brain samples were then treated with either 20

443 mM D-glucose or 1 mM of chemically synthesized peptides dissolved in HL3.1 buffer

444 for 5 min. After incubation, samples were subjected to immunohistochemical analyses
445 to visualize GFP, mCherry, and anti-Dilp3 signals (see the section
446 "Immunohistochemistry").
447 Image processing was performed using ImageJ v1.53t ((Schneider et al., 2012);
448 RRID:SCR_003070). Nuclear ROIs and cell body outlines were determined based on
449 the mCD8::mCherry fluorescence insensitive to neuronal activity, and the mean
450 intensities of CRTC::GFP signals within the nucleus (F_{nuc}) and the cytoplasm (F_{cyto} =
451 $F_{whole\ cell}$ - F_{nuc}) were quantified. NLI was calculated using the following formula: (F_{nuc} -
452 F_{cyto})/(F_{nuc} + F_{cyto}). To assess Dilp3 accumulation in IPCs, the anti-Dilp3 signal intensity
453 was measured within the cytosol of each cell, excluding the nucleus. Data from 4–14
454 Dilp3-positive IPCs per brain, collected from 3–7 larvae, were pooled for each
455 genotype/treatment group.
456
457 **Chemical synthesis of Hug peptides**
458 Peptides with the following amino acid sequences were chemically synthesized using
459 the Fmoc solid phase method, and their purity was assessed by HPLC to be over 95%.
460 All procedures were carried out by Eurofins Genomics K.K. (Tokyo, Japan). The amino
461 acid sequences of the peptides used were as follows:
462 *Drosophila* Hug-γ:
463 Acetyl-QLQSNGEPAYRVRTPRL-CONH2 (17 a.a.)
464 *Drosophila* PK-2:
465 Acetyl-SVPFKPRL-CONH2 (8 a.a.)
466 Human NMU:
467 Acetyl-FRVDEEFQSPFASQSRGYFLFRPRN-CONH2 (25 a.a.)

468

469 **Sleep quantification in adult flies**

470 The following parts of the *Drosophila* activity monitor (DAM) system were purchased
471 from TriKinetics Inc. (Waltham, MA): the *Drosophila* Activity Monitor (cat# DAM2),
472 the power supply interface unit (cat# PSIU9), monitor tubes with an outside diameter of
473 5 mm and a length of 65 mm (cat# PGT5x65), and tube caps (cat# CAP5-Black). Newly
474 eclosed adult flies were collected under brief CO_2 anesthesia and kept as groups of 10–
475 15 in standard food vials. Males and females were kept separately to avoid mating. To
476 minimize disturbance by noise and vibration, flies were placed inside a fan-less Peltier-
477 type incubator (Mitsubishi Electric Engineering Co., Ltd., cat# SLC-25) set to 25°C,
478 externally connected with 5-mm diameter LED lights (MY-CRAFT, Ltd., cat# 5W0601)
479 and a timer device (Panasonic Corp., cat# WH3311WP) to generate a 9AM:9PM
480 light/dark cycle. After 3 days of eclosion, each fly was gently aspirated into a Pyrex
481 glass monitor tube, one end of which was stuffed with agar food (2% (w/w) agar and
482 5% (w/w) sucrose), and the other was plugged with a cotton string. The tubes were set
483 to the monitor device and placed inside the same fan-less incubator. The DAM system
484 was connected to an external PC running DAMSystem3 Data Collection Software
485 (RRID:SCR_021809; available at https://trikinetics.com/), which counted beam-
486 crossings by each fly for two successive days. Time windows longer than 5 min without
487 beam-crossing were judged as sleep bouts, following the conventional criteria for adult
488 fly sleep (Paul et al., 2000).

489

490 **Statistical analysis**

491 Statistical analyses by Kruskal–Wallis one-way ANOVA, Mann–Whitney U-test, or chi-

492 squared test were performed using Prism 9.5.1 (GraphPad, RRID:SCR_002798).
493 Bonferroni correction was applied for multiple comparisons. Asterisks (*) represent p-
494 values as indicated within each figure legend. All data necessary to reproduce the figure
495 panels and statistical analyses are available as Source Data files.
496

497 **Acknowledgements**

498 We thank Y. Rao, M. Pankratz, S. Waddel, and the Bloomington *Drosophila* Stock
499 Center for fly stocks; J. A. Veenstra for the anti-Dilp3 antibody; T. Nishimura for the
500 anti-Dilp2 antibody; Y. Nishizuka for valuable suggestions on writing codes for
501 automated larval detection and sleep quantification; H. Ito, N. Yamaji, M. Maetani, A.
502 Ogasawara, E. Kato, T. Rikiishi, S. Ando, M. Hayashi, and S. Miyazaki for technical
503 assistance and fly maintenance; and the members of Emoto Lab for critical comments
504 and discussion. This work is supported by MEXT Grants-in-Aid for Scientific Research
505 on Innovative Areas "Dynamic regulation of brain function by Scrap and Build system"
506 (KAKENHI 16H06456), JSPS (KAKENHI 16H02504), WPI-IRCN, AMED-CREST
507 (JP22gm310010), JSTCREST, Toray Foundation, Naito Foundation, Takeda Science
508 Foundation, and Uehara Memorial Foundation to K.E.; the Leading Initiative for
509 Excellent Young Researchers (LEADER) from MEXT, JSPS (KAKENHI 22K06309),
510 and AMED-PRIME (JP22gm6510011) to K.I.; Grant-in-Aid for JSPS Fellows
511 (24KJ0911) to M.M.; and Grant-in-Aid for JSPS Fellows (22J21096; 22KJ1042) to
512 C.H.
513

514 **Author contributions**

C.H., K.I., and M.M. performed experiments and data analyses; M.T. wrote the codes for automated larval detection and sleep quantification; C.H., K.I., and K.E. are responsible for study conception, experimental design, and data interpretation; C.H., K.I., and K.E. wrote the original manuscript, and M.T. edited the paper.

Competing interests

The authors declare no conflicts of interest.

523 **Figure legends**

524 **Figure 1. PK2-R1 is required for larval sleep control**

525 (A) Sleep amounts in *PK2-R1* or *Oamb* knock-out mutants. In this and the following
526 panels, 'N' indicates the number of biologically independent animals used for each
527 group. Box plots are generated so that the center line indicates the median, the box
528 limits indicate the upper and lower quartiles, and the whiskers indicate the minimum-to-
529 maximum range. *** $p < 0.001$ (Mann–Whitney U-test with Bonferroni correction). (B)
530 Sleep amounts in larvae in which *PK2-R1* neurons were silenced. *** $p < 0.001$ (Mann–
531 Whitney U-test with Bonferroni correction). (C) The expression pattern of *PK2-R1*$^{2A\text{-}GAL4}$ > *UAS-Kir2.1::EGFP* in the larval CNS. Similar results were obtained across three
533 independent samples.
534

535 **Figure 1—figure supplement 1. Detailed experimental setup for analyzing larval**
536 **sleep**

537 (A) Schematic flow of automated larval sleep quantification. A second instar larva was
538 placed in each of 24 wells, and all 24 wells were videotaped from above. For each well
539 and frame, the image of larva was blurred and binarized to automatically locate the
540 larva. Consecutive frames were then compared so that changes in pixel values were
541 summed to estimate larval motion. This motion estimate was then used to classify every
542 consecutive pair of frames as representing "active" or "inactive." We found that
543 inactivity across 12 consecutive frames meets the sleep criteria, as shown in Figure 1—
544 figure supplement 2. (B) Schematic representation of the 24-well chamber used for
545 larval sleep assays. (C) Flow of automated processes of larval motion detection and
546 active/inactive state determination. For each well and frame, the image of larva was

547 blurred and binarized. Consecutive frames were then compared so that changes in pixel
548 values were summed to estimate larval motion. This motion estimate was then used to
549 classify every consecutive pair of frames as representing “active” or “inactive.”
550
551 **Figure 1—figure supplement 2. Larval “sleep state” in this study is consistent with**
552 **behavioral criteria for sleep**
553 (A) Relationship between “inactive” state duration and spontaneous arousal probability.
554 Sustained quiescence for ≥ 12 frames (open circles) significantly reduced arousal
555 probability compared to 1-frame inactivity. * $p < 0.05$, NS: $p \geq 0.05$ (chi-squared test).
556 (B) The percentage of larvae that showed a response within the next 10 frames after
557 high-intensity blue light. The number of events analyzed was 36 and 60 with and
558 without blue light irradiation, respectively. * $p < 0.05$ (Fisher’s exact test). (C) Sleep
559 amounts before, during, and after blue light irradiation. The number of larvae tested was
560 21 and 21 for the control and experimental groups, respectively. ** $p < 0.01$, NS: $p \geq$
561 0.05 (Mann–Whitney U-test with Bonferroni correction). (D) Percentage of larvae that
562 showed a response in the next 1 or 12 frames after blue light stimulation. Number of
563 events analyzed: 1960 or 111 for 1- or 12-frame continuous inactivity prior to blue light
564 illumination, respectively. **** $p < 0.0001$ (chi-squared test).
565
566 **Figure 1—figure supplement 3. CRISPR-knock-out screen for genes that regulate**
567 **larval sleep.**
568 Total sleep amounts in CRISPR-knock-out mutants were measured for 18 h from the
569 beginning of the second instar. The data for Control, *PK2-R1,* and *Oamb* mutants are
570 identical to those shown in Figure 1. Box plots are generated so that the center line

571 indicates the median, the box limits indicate the upper and lower quartiles, and the
572 whiskers indicate the minimum-to-maximum range. *** $p < 0.005$ (Kruskal–Wallis one-
573 way ANOVA and post hoc Mann–Whitney U-test with Bonferroni correction). Number
574 of larvae tested: 475 for the control and 10–52 for each mutant.
575
576 **Figure 1—figure supplement 4. Effects of neuronal manipulation on larval sleep**
577 Sleep amounts in larvae in which distinct neuronal populations were silenced. Kir2.1
578 expression was driven by each enhancer-GAL4 for "hit" genes identified in the
579 CRISPR-knock-out screen. 'N' indicates the number of biologically independent
580 animals used for each group. Box plots are generated so that the center line indicates the
581 median, the box limits indicate the upper and lower quartiles, and the whiskers indicate
582 the minimum-to-maximum range. *** $p < 0.001$, ** $p < 0.01$, * $p < 0.05$, NS: ≥ 0.05
583 (Mann–Whitney U-test with Bonferroni correction).
584
585 **Figure 2. IPCs and Dilps negatively regulate larval sleep**
586 (A) Triple labeling of *PK2-R1* neurons expressing nuclear-localized RFP (magenta),
587 *Dilp3* neurons expressing nuclear-localized GFP (green), and anti-Dilp2 positive cells
588 (blue). Top panels show signals in the larval brain and the VNC. The bottom panels
589 show magnified images of the white-squared area in the top panels, where the cell
590 bodies of the IPCs are located. Note that all IPCs labeled by *Dilp3-GAL4* are also
591 labeled by $PK2\text{-}R1^{2A\text{-}LexA}$. Similar results were obtained across five independent
592 samples. (B) Triple labeling of *PK2-R1* neurons expressing nuclear-localized RFP
593 (magenta), *Dilp5* neurons expressing nuclear-localized GFP (green), and anti-Dilp2
594 positive cells (blue). Similar results were obtained across five independent samples. (C)

595 Effect of IPCs silencing on larval sleep. In this and the following panels, 'N' indicates
596 the number of biologically independent animals used for each group. Box plots are
597 generated so that the center line indicates the median, the box limits indicate the upper
598 and lower quartiles, and the whiskers indicate the minimum-to-maximum range. *** p
599 < 0.001, ** $p < 0.01$, * $p < 0.05$ (Mann–Whitney U-test with Bonferroni correction).
600 (D) Sleep amounts in *Dilp3* or *Dilp5* null mutant larvae. *** $p < 0.001$, ** $p < 0.01$
601 (Mann–Whitney U-test with Bonferroni correction).
602
603 **Figure 2—figure supplement 1. Locomotion speeds are not consistently affected by**
604 **genetical manipulations of *PK2-R1*, IPCs, or *Dilps***
605 (A–B) Effects of silencing *PK2-R1* neurons (A) and IPCs (B) on larval locomotion
606 speed. (C) Larval locomotion speed in null mutants of *Dilp3* or *Dilp5*. The average
607 locomotion speed during the wake periods was measured from the data presented in
608 Figures 1B, 2C, and 2D. In this and the following panels, 'N' indicates the number of
609 biologically independent animals used for each group. Box plots are generated so that
610 the center line indicates the median, the box limits indicate the upper and lower
611 quartiles, and the whiskers indicate the minimum-to-maximum range. *** $p < 0.0001$, *
612 $p < 0.05$, NS: $p \geq 0.05$ (Mann–Whitney U-test with Bonferroni correction).
613
614 **Figure 3. *Hug* neurons negatively regulate larval sleep**
615 (A) Sleep amounts in *Hug* CRISPR-knock-out mutant larvae. In this and the following
616 panels, 'N' indicates the number of biologically independent animals used for each
617 group. Box plots are generated so that the center line indicates the median, the box
618 limits indicate the upper and lower quartiles, and the whiskers indicate the minimum-to-

619 maximum range. **** $p < 0.0001$ (Mann–Whitney U-test). (B) Effect of silencing *Hug*
620 neurons on larval sleep amount. *** $p < 0.001$ (Mann–Whitney U-test with Bonferroni
621 correction). (C) Larval sleep changes induced by optogenetic activation of *Hug* neurons.
622 For each genotype, sleep duration in the 1-h light-ON period was normalized to that in
623 the 1-h light-OFF phase. * $p < 0.05$ (Mann–Whitney U-test). (D) Larval sleep during
624 thermogenetic activation of *Hug* neurons. *** $p < 0.001$ (Mann–Whitney U-test with
625 Bonferroni correction). (E) Images of HugPC neurons and IPCs labeled by rCD2::RFP
626 (magenta) and mCD8::GFP (green), respectively. The bottom panels show magnified
627 images of the white-squared region in the top panels, in which HugPC neurons project
628 their axons close to the cell bodies of the IPCs. While the top panels are z-stacks of 122
629 image slices (1 μm interval) covering the entire brain, the bottom panels are projections
630 of 60 slices around the cell bodies of IPCs. Similar results were obtained across five
631 independent samples. (F) Effect of silencing HugPC neurons on larval sleep. *** $p <$
632 0.001, ** $p < 0.01$ (Mann–Whitney U-test with Bonferroni correction).
633
634 **Figure 3—figure supplement 1. Neither *Hug* knock-out mutation nor *Hug* neuron**
635 **silencing significantly affects larval locomotion speed**
636 (A) Average locomotion speed of *Hug* knock-out mutants during waking periods. The
637 data presented in Figures 3A and 3B were reanalyzed. In this and the following panels,
638 'N' indicates the number of biologically independent animals used for each group. Box
639 plots are generated so that the center line indicates the median, the box limits indicate
640 the upper and lower quartiles, and the whiskers indicate the minimum-to-maximum
641 range. NS: $p \geq 0.05$ (Mann–Whitney U-test). (B) Locomotion speed of larvae in which
642 *Hug* neurons were silenced. NS: $p \geq 0.05$ (Mann–Whitney U-test with Bonferroni

643 correction).

644

645 **Figure 3—figure supplement 2. Generation of *HugPC-LexA* transgenic lines**

646 (A–D) Labeling patterns of four *HugPC-LexA* strains in larval CNS visualized by

647 rCD2::RFP. These transgenic lines were generated by injecting the identical plasmid

648 into the following landing sites, respectively: su(Hw)attP5, VK00005, attP2, and attP40.

649 Arrowheads indicate cell bodies of non-HugPC neurons. Filled and unfilled arrowheads

650 indicate cell bodies within the VNC and near the protocerebrum, respectively.

651

652 **Figure 4. Activation of *Hug* neurons triggers Ca^{2+} responses in larval IPCs**

653 (A) Schematic flow of assessing intracellular Ca^{2+} levels in IPCs while performing the

654 thermogenetic activation of *Hug* neurons. (B–C) The level of nuclear-localized

655 CRTC::GFP signal, calculated as NLI (see the Methods section for a detailed explanation

656 of NLI), in IPCs during *Hug* neurons stimulation *ex vivo* (B) or *in vivo* (C). In these panels,

657 'N' indicates the number of cells used for each group. Box plots are generated so that the

658 center line indicates the median, the box limits indicate the upper and lower quartiles, and

659 the whiskers indicate the minimum-to-maximum range. **** $p < 0.0001$ (Mann–Whitney

660 U-test). (D) The proposed neuronal connection that regulates larval sleep.

661

662 **Figure 5. Hug peptides induce Ca^{2+} responses in larval IPCs via PK2-R1**

663 (A) Schematic flow of assessing intracellular Ca^{2+} levels in IPCs and bath application of

664 peptides. (B–C) Ca^{2+} responses in IPCs to *ex vivo* bath application of either glucose (B)

665 or Hug peptides (C). In this and the following panels, 'N' indicates the number of cells

666 used for each group. Box plots are generated so that the center line indicates the median,

667 the box limits indicate the upper and lower quartiles, and the whiskers indicate the
668 minimum-to-maximum range. **** $p < 0.0001$, *** $p < 0.001$ (Mann–Whitney U-test
669 with Bonferroni correction). (D) Representative images of larval IPCs after peptide
670 application. Scale bars, 2 μm. (E) Anti-Dilp3 signal intensity measured within the
671 cytosolic areas of IPCs. *** $p < 0.001$, * $p < 0.05$ (Mann–Whitney U-test with
672 Bonferroni correction). (F–G) Ca^{2+} responses in IPCs of *PK2-R1* knock-out mutants,
673 measured following either glucose (F) or Hug peptide application (G). ** $p < 0.01$, NS:
674 $p \geq 0.05$ (Mann–Whitney U-test with Bonferroni correction). (H) A model where Hug
675 peptides, but not glucose, activate IPCs via the PK2-R1 receptor.
676

677 **Figure 5—figure supplement 1. D-glucose but not Hug peptide cause Dilp2**
678 **reduction in IPCs**

679 (A–B) Anti-Dilp2 signal intensity measured in IPCs after glucose (A) or Hug-γ
680 application (B). In this and the following panels, 'N' indicates the number of cells used
681 for each group. Box plots are generated so that center line indicates median, box limits
682 indicate upper and lower quartiles, and whiskers indicate the minimum-to-maximum
683 range. **** $p < 0.0001$, * $p < 0.05$ (Mann–Whitney U-test). (C) Anti-Dilp3 signal
684 intensity measured within the cytosolic areas of IPCs. NS: ≥ 0.05 (Mann–Whitney U-
685 test).
686

687 **Figure 6. Distinct impacts of Hugin/PK2-R1 axis on wake/sleep control in larvae**
688 **and adults**

689 (A) Total sleep amounts in *Hug* knock-out mutant adults. NS: $p \geq 0.05$ (Mann–Whitney

690 U-test). In these and the following panels, 'N' indicates the number of biologically
691 independent animals used for each group. Box plots are generated so that the center line
692 indicates the median, the box limits indicate the upper and lower quartiles, and the
693 whiskers indicate the minimum-to-maximum range. NS: $p \geq 0.05$ (Mann–Whitney U-
694 test). (B) Sleep amounts of adults in which HugPC neurons were silenced. *** $p <$
695 0.001, NS: $p \geq 0.05$ (Mann–Whitney U-test with Bonferroni correction). (C) Sleep
696 amounts in *Dilp3* or *Dilp5* null mutant adults. *** $p < 0.001$ (Mann–Whitney U-test
697 with Bonferroni correction). (D) Schematic flow of peptide application experiments
698 using adult brains. (E–F) Ca^{2+} responses (E) and anti-Dilp3 signal intensity (F) in adult
699 IPCs after Hug peptide application. ** $p < 0.01$, NS: $p \geq 0.05$ (Mann–Whitney U-test
700 with Bonferroni correction).
701

702 **Figure 6—figure supplement 1. Sleep patterns of adult flies following**
703 **manipulations of Hugin and insulin pathways**

704 (A) Experimental setup for monitoring adult sleep using the *Drosophila* Activity
705 Monitor (DAM). (B) Sleep duration in adult CRISPR-knock-out mutants. These
706 mutants showed significant changes in the sleep amounts in larvae (Figure 1—figure
707 supplement 3). In panels B, C, and E, sleep amounts were calculated as the ratio relative
708 to the median sleep amount of the control group. Box plots are generated so that the
709 center line indicates the median, the box limits indicate the upper and lower quartiles,
710 and the whiskers indicate the minimum-to-maximum range. *** $p < 0.001$, ** $p < 0.01$
711 (Kruskal–Wallis one-way ANOVA and post hoc Mann–Whitney U-test with Bonferroni
712 correction). (C, E) Sleep amounts relative to the median value of the control group. Data
713 presented in Figures 6B and 6C were reanalyzed. *** $p < 0.001$, * $p < 0.05$, NS: $p \geq$

714 0.05 (Mann–Whitney U-test with Bonferroni correction). (D, F) Temporal sleep patterns
715 over two consecutive days.
716
717 **Figure 6—figure supplement 2. Morphology of *PK2-R1* neurons, HugPC neurons,**
718 **and IPCs in the adult brain**
719 (A) Dual labeling of *PK2-R1* neurons and IPCs expressing nuclear-localized RFP
720 (stinger; magenta) and GFP (stinger; green), respectively. The top panels show signals
721 in the entire adult brain. The bottom panels show magnified images of the white-
722 squared area in each corresponding top panel, where the cell bodies of IPCs are located.
723 Similar results were obtained across five independent samples. (B) Visualization of
724 HugPC neurons and IPCs labeled by mCD8::GFP (magenta) and the anti-Dilp3
725 antibody (green), respectively. Similar results were obtained across four independent
726 samples.
727
728 **Figure 7. A schematic model of the Hugin/PK2-R1/Dilps axis in larval and adult**
729 **sleep regulation**
730

References

Ahnaou, A., & Drinkenburg, W. H. I. M. (2011). Neuromedin U2 receptor signaling mediates alteration of sleep-wake architecture in rats. *Neuropeptides*, 45(2), 165–174. Retrieved from https://doi.org/10.1016/j.npep.2011.01.004

Bader, R., Colomb, J., Pankratz, B., Schröck, A., Stocker, R. F., & Pankratz, M. J. (2007). Genetic dissection of neural circuit anatomy underlying feeding behavior in Drosophila: Distinct classes of hugin-expressing neurons. *Journal of Comparative Neurology*, 502(5), 848–856. Retrieved from https://doi.org/10.1002/cne.21342

Baines, R. A., Uhler, J. P., Thompson, A., Sweeney, S. T., & Bate, M. (2001). *Altered Electrical Properties in Drosophila Neurons Developing without Synaptic Transmission*.

Barlow, I. L., & Rihel, J. (2017, June 1). Zebrafish sleep: from geneZZZ to neuronZZZ. *Current Opinion in Neurobiology*. Elsevier Ltd. Retrieved from https://doi.org/10.1016/j.conb.2017.02.009

Blumberg, M. S., H Seelke, A. M., Lowen, S. B., & Karlsson, K. A. (2005). Dynamics of sleep–wake cyclicity in developing rats. *PNAS*, 102(41). Retrieved from www.pnas.orgcgidoi10.1073pnas.0506340102

Bonheur, M., Swartz, K. J., Metcalf, M. G., Wen, X., Zhukovskaya, A., Mehta, A., … Hattori, D. (2023). A rapid and bidirectional reporter of neural activity reveals neural correlates of social behaviors in Drosophila. *Nature Neuroscience*, 26(7), 1295–1307. Retrieved from https://doi.org/10.1038/s41593-023-01357-w

Burke, C. J., Huetteroth, W., Owald, D., Perisse, E., Krashes, M. J., Das, G., … Waddell, S. (2012). Layered reward signalling through octopamine and dopamine in Drosophila. *Nature*, 492(7429), 433–437. Retrieved from https://doi.org/10.1038/nature11614

Chiu, C. N., Rihel, J., Lee, D. A., Singh, C., Mosser, E. A., Chen, S., … Prober, D. A. (2016). A Zebrafish Genetic Screen Identifies Neuromedin U as a Regulator of Sleep/Wake States. *Neuron*, 89(4), 842–856. Retrieved from https://doi.org/10.1016/j.neuron.2016.01.007

Churgin, M. A., Szuperak, M., Davis, K. C., Raizen, D. M., Fang-Yen, C., & Kayser, M. S. (2019). Quantitative imaging of sleep behavior in Caenorhabditis elegans and larval Drosophila melanogaster. *Nature Protocols 2019 14:5*, 14(5), 1455–1488. Retrieved 25 December 2021 from https://doi.org/10.1038/s41596-019-0146-6

Davis, K. F., Parker, K. P., & Montgomery, G. L. (2004). *Sleep in infants and young children: Part one: normal sleep*. *Journal of Pediatric Health Care* (Vol. 18, pp. 65–71). Mosby. Retrieved 25 December 2021 from https://doi.org/10.1016/S0891-5245(03)00149-4

Deng, B., Li, Q., Liu, X., Cao, Y., Li, B., Qian, Y., … Rao, Y. (2019). Chemoconnectomics: Mapping Chemical Transmission in Drosophila. *Neuron*, 101(5), 876-893.e4. Retrieved from https://doi.org/10.1016/j.neuron.2019.01.045

Dubowy, C., & Sehgal, A. (2017). Circadian rhythms and sleep in Drosophila melanogaster. *Genetics*, 205(4), 1373–1397. Retrieved from https://doi.org/10.1534/genetics.115.185157

Enell, L. E., Kapan, N., Söderberg, J. A. E., Kahsai, L., & Nässe, D. R. (2010). Insulin signaling, lifespan and stress resistance are modulated by metabotropic GABA receptors on insulin producing cells in the brain of Drosophila. *PLoS ONE*, 5(12). Retrieved from https://doi.org/10.1371/journal.pone.0015780

Frank, M. G., Ruby, N. F., Heller, H. C., & Franken, P. (2017). Development of circadian sleep regulation in the rat: A longitudinal study under constant conditions. *Sleep*, 40(3). Retrieved from https://doi.org/10.1093/sleep/zsw077

Géminard, C., Rulifson, E. J., & Léopold, P. (2009). Remote Control of Insulin Secretion by Fat Cells in Drosophila. *Cell Metabolism*, 10(3), 199–207. Retrieved from https://doi.org/10.1016/j.cmet.2009.08.002

Groth, A. C., Fish, M., Nusse, R., & Calos, M. P. (2004). Construction of Transgenic Drosophila by Using the Site-Specific Integrase From Phage φC31. *Genetics*, (166), 1775–1782. Retrieved from https://academic.oup.com/genetics/article/166/4/1775/6052665

Hamada, F. N., Rosenzweig, M., Kang, K., Pulver, S. R., Ghezzi, A., Jegla, T. J., & Garrity, P. A. (2008). An internal thermal sensor controlling temperature preference in Drosophila. *Nature*, 454(7201), 217–220. Retrieved from https://doi.org/10.1038/nature07001

Hendricks, J. C., Lu, S., Kume, K., Yin, J. C. P., Yang, Z., & Sehgal, A. (2003). Gender dimorphism in the role of cycle (BMAL1) in rest, rest regulation, and longevity in Drosophila melanogaster. *Journal of Biological Rhythms*, 18(1), 12–25. Retrieved from https://doi.org/10.1177/0748730402239673

Hückesfeld, S., Peters, M., & Pankratz, M. J. (2016). Central relay of bitter taste to the protocerebrum by peptidergic interneurons in the Drosophila brain. *Nature*

Communications, 7. Retrieved from https://doi.org/10.1038/ncomms12796

Hückesfeld, S., Schlegel, P., Miroschnikow, A., Schoofs, A., Zinke, I., Haubrich, A. N., … Pankratz, M. J. (2021). Unveiling the sensory and interneuronal pathways of the neuroendocrine connectome in Drosophila. *ELife*. Retrieved from https://doi.org/10.7554/eLife

Inagaki, H. K., Jung, Y., Hoopfer, E. D., Wong, A. M., Mishra, N., Lin, J. Y., … Anderson, D. J. (2014). Optogenetic control of Drosophila using a red-shifted channelrhodopsin reveals experience-dependent influences on courtship. *Nature Methods*, 11(3), 325–332. Retrieved from https://doi.org/10.1038/nmeth.2765

Kauffman, M. R., & DiAngelo, J. R. (2024). Glut1 Functions in Insulin-Producing Neurons to Regulate Lipid and Carbohydrate Storage in Drosophila. *Biomolecules*, 14(8). Retrieved from https://doi.org/10.3390/biom14081037

Kréneisz, O., Chen, X., Fridell, Y. W. C., & Mulkey, D. K. (2010). Glucose increases activity and Ca2+ in insulin-producing cells of adult Drosophila. *NeuroReport*, 21(17), 1116–1120. Retrieved from https://doi.org/10.1097/WNR.0b013e3283409200

Kume, K., Kume, S., Park, S. K., Hirsh, J., & Jackson, F. R. (2005). Dopamine Is a Regulator of Arousal in the Fruit Fly. *Journal of Neuroscience*, 25(32), 7377–7384. Retrieved 10 December 2024 from https://doi.org/10.1523/JNEUROSCI.2048-05.2005

Nakamizo-Dojo, M., Ishii, K., Yoshino, J., Tsuji, M., & Emoto, K. (2023). Descending GABAergic pathway links brain sugar-sensing to peripheral nociceptive gating in Drosophila. *Nature Communications*, 14(1). Retrieved from https://doi.org/10.1038/s41467-023-42202-9

Nässel, D. R., Liu, Y., & Luo, J. (2015). Insulin/IGF signaling and its regulation in Drosophila. *General and Comparative Endocrinology*, 221, 255–266. Retrieved from https://doi.org/10.1016/j.ygcen.2014.11.021

Oh, Y., Lai, J. S. Y., Mills, H. J., Erdjument-Bromage, H., Giammarinaro, B., Saadipour, K., … Suh, G. S. B. (2019). A glucose-sensing neuron pair regulates insulin and glucagon in Drosophila. *Nature*, 574(7779), 559–564. Retrieved from https://doi.org/10.1038/s41586-019-1675-4

Ohhara, Y., Blick, M., Park, D., Yoon, S. E., Kim, Y. J., Pankratz, M. J., … Yamanaka, N. (2024). A Neuropeptide Signaling Network That Regulates Developmental Timing and Systemic Growth in Drosophila. *The Journal of Comparative*

Neurology, 532(10), e25677. Retrieved from https://doi.org/10.1002/cne.25677

Okamoto, N. (2021). Insect insulin-like peptides. In *Handbook of Hormones: Comparative Endocrinology for Basic and Clinical Research* (pp. 673–675). Elsevier. Retrieved from https://doi.org/10.1016/B978-0-12-820649-2.00177-7

Okamoto, N., Nakamori, R., Murai, T., Yamauchi, Y., Masuda, A., & Nishimura, T. (2013). A secreted decoy of InR antagonizes insulin/IGF signaling to restrict body growth in drosophila. *Genes and Development*, 27(1), 87–97. Retrieved from https://doi.org/10.1101/gad.204479.112

Okamoto, N., Nishimori, Y., & Nishimura, T. (2012). Conserved role for the Dachshund protein with Drosophila Pax6 homolog eyeless in insulin expression. *Proceedings of the National Academy of Sciences of the United States of America*, 109(7), 2406–2411. Retrieved from https://doi.org/10.1073/pnas.1116050109

Paul J. Shaw, Chiara Cirelli, Ralph J. Greenspan, & Giulio Tononi. (2000). Correlates of Sleep and Waking in Drosophila melanogaster. *SCIENCE*, (287), 1834–1837.

Poe, A. R., Zhu, L., Szuperak, M., Mcclanahan, P. D., Anafi, R. C., Scholl, B., … Kayser, M. S. (2023). *Developmental emergence of sleep rhythms enables long-term memory in Drosophila*. Retrieved from https://www.science.org

Raizen, D. M., Zimmerman, J. E., Maycock, M. H., Ta, U. D., You, Y. J., Sundaram, M. V., & Pack, A. I. (2008). Lethargus is a Caenorhabditis elegans sleep-like state. *Nature*, 451(7178), 569–572. Retrieved from https://doi.org/10.1038/nature06535

Rosenkilde, C., Cazzamali, G., Williamson, M., Hauser, F., Søndergaard, L., DeLotto, R., & Grimmelikhuijzen, C. J. P. (2003). Molecular cloning, functional expression, and gene silencing of two Drosophila receptors for the Drosophila neuropeptide pyrokinin-2. *Biochemical and Biophysical Research Communications*, 309(2), 485–494. Retrieved from https://doi.org/10.1016/j.bbrc.2003.08.022

Scammell, T. E., Arrigoni, E., & Lipton, J. O. (2017, February 22). Neural Circuitry of Wakefulness and Sleep. *Neuron*. Cell Press. Retrieved from https://doi.org/10.1016/j.neuron.2017.01.014

Schlegel, P., Texada, M. J., Miroschnikow, A., Schoofs, A., Hückesfeld, S., Peters, M., … Pankratz, M. J. (2016a). Synaptic transmission parallels neuromodulation in a central food-intake circuit. *ELife*, 5(NOVEMBER2016).

Retrieved from https://doi.org/10.7554/eLife.16799.001

Schlegel, P., Texada, M. J., Miroschnikow, A., Schoofs, A., Hückesfeld, S., Peters, M., … Pankratz, M. J. (2016b). Synaptic transmission parallels neuromodulation in a central food-intake circuit. *ELife*, 5(NOVEMBER2016). Retrieved from https://doi.org/10.7554/eLife.16799.001

Schneider, C. A., Rasband, W. S., & Eliceiri, K. W. (2012). NIH Image to ImageJ: 25 years of image analysis. *Nature Methods*, 9(7), 671–675. Retrieved from https://doi.org/10.1038/nmeth.2089

Schoofs, A., Hückesfeld, S., Schlegel, P., Miroschnikow, A., Peters, M., Zeymer, M., … Pankratz, M. J. (2014). Selection of Motor Programs for Suppressing Food Intake and Inducing Locomotion in the Drosophila Brain. *PLoS Biology*, 12(6). Retrieved from https://doi.org/10.1371/journal.pbio.1001893

Schwarz, J. E., King, A. N., Hsu, C. T., Barber, A. F., & Sehgal, A. (2021). Hugin + neurons provide a link between sleep homeostat and circadian clock neurons. *PNAS*. Retrieved from https://doi.org/10.1073/pnas.2111183118/-/DCSupplemental

Shafer, O. T., & Keene, A. C. (2021, January 11). The Regulation of Drosophila Sleep. *Current Biology*. Cell Press. Retrieved from https://doi.org/10.1016/j.cub.2020.10.082

Sorribes, A., Porsteinsson, H., Arnardóttir, H., Jóhannesdóttir, I. P., Sigurgeirsson, B., de Polavieja, G. G., & Karlsson, K. (2013). The ontogeny of sleep-wake cycles in zebrafish: A comparison to humans. *Frontiers in Neural Circuits*, 7(NOV). Retrieved from https://doi.org/10.3389/fncir.2013.00178

Szuperak, M., Churgin, M. A., Borja, A. J., Raizen, D. M., Fang-Yen, C., & Kayser, M. S. (2018a). A sleep state in Drosophila larvae required for neural stem cell proliferation. *ELife*, 7. Retrieved 25 December 2021 from https://doi.org/10.7554/ELIFE.33220

Szuperak, M., Churgin, M. A., Borja, A. J., Raizen, D. M., Fang-Yen, C., & Kayser, M. S. (2018b). A sleep state in Drosophila larvae required for neural stem cell proliferation. *ELife*. Retrieved from https://doi.org/10.7554/eLife.33220.001

Tomoatsu Ikeya, Milos Galic, Priyanka Belawat, Knud Nairz, & Ernst Hafen. (2002). *Nutrient-Dependent Expression of Insulin-like Peptides from Neuroendocrine Cells in the CNS Contributes to Growth Regulation in Drosophila median neurosecretory cells (m-NSCs) possessing axon*.

Veenstra, J. A., Agricola, H. J., & Sellami, A. (2008). Regulatory peptides in fruit fly

midgut. *Cell and Tissue Research*, 334(3), 499–516. Retrieved from https://doi.org/10.1007/s00441-008-0708-3

915 **Figures**

916

Figure 1

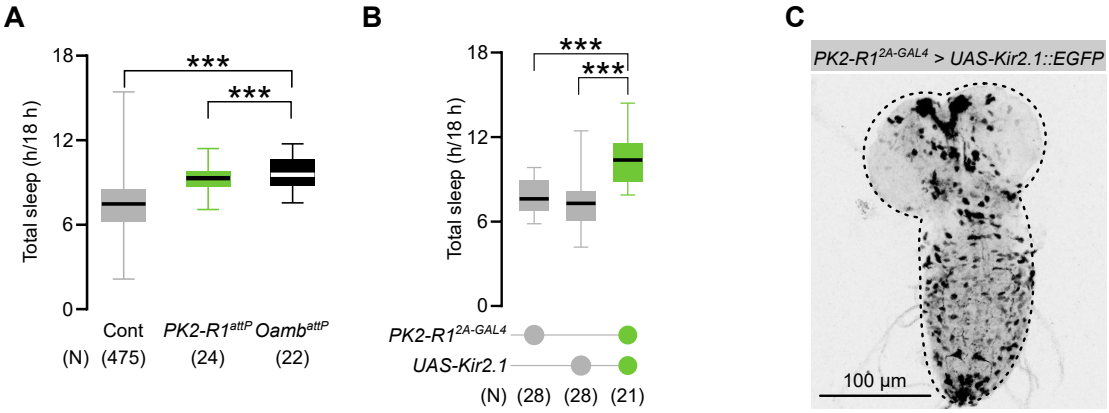

917

918 **Figure 1. PK2-R1 is required for larval sleep control**

919 (A) Sleep amounts in *PK2-R1* or *Oamb* knock-out mutants. In this and the following
920 panels, 'N' indicates the number of biologically independent animals used for each
921 group. Box plots are generated so that the center line indicates the median, the box
922 limits indicate the upper and lower quartiles, and the whiskers indicate the minimum-to-
923 maximum range. *** $p < 0.001$ (Mann–Whitney U-test with Bonferroni correction). (B)
924 Sleep amounts in larvae in which *PK2-R1* neurons were silenced. *** $p < 0.001$ (Mann–
925 Whitney U-test with Bonferroni correction). (C) The expression pattern of *PK2-R1*$^{2A-GAL4}$ > *UAS-Kir2.1::EGFP* in the larval CNS. Similar results were obtained across three
927 independent samples.

928

Figure 1—figure supplement 1

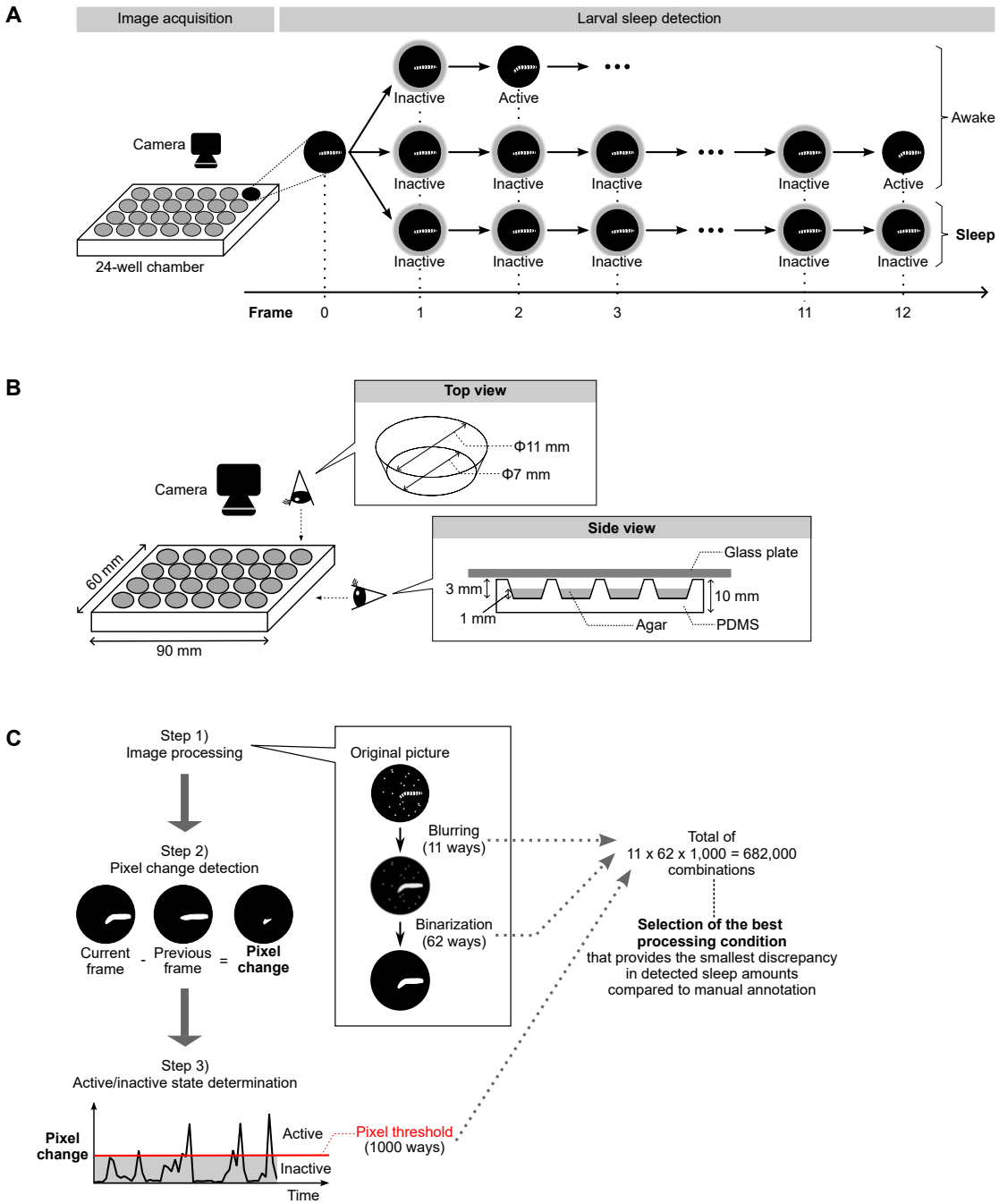

Figure 1—figure supplement 1. Detailed experimental setup for analyzing larval sleep

(A) Schematic flow of automated larval sleep quantification. A second instar larva was placed in each of 24 wells, and all 24 wells were videotaped from above. For each well and frame, the image of larva was blurred and binarized to automatically locate the larva. Consecutive frames were then compared so that changes in pixel values were summed to estimate larval motion. This motion estimate was then used to classify every

consecutive pair of frames as representing “active” or “inactive.” We found that inactivity across 12 consecutive frames meets the sleep criteria, as shown in Figure 1—figure supplement 2. (B) Schematic representation of the 24-well chamber used for larval sleep assays. (C) Flow of automated processes of larval motion detection and active/inactive state determination. For each well and frame, the image of larva was blurred and binarized. Consecutive frames were then compared so that changes in pixel values were summed to estimate larval motion. This motion estimate was then used to classify every consecutive pair of frames as representing “active” or “inactive.”

Figure 1—figure supplement 2

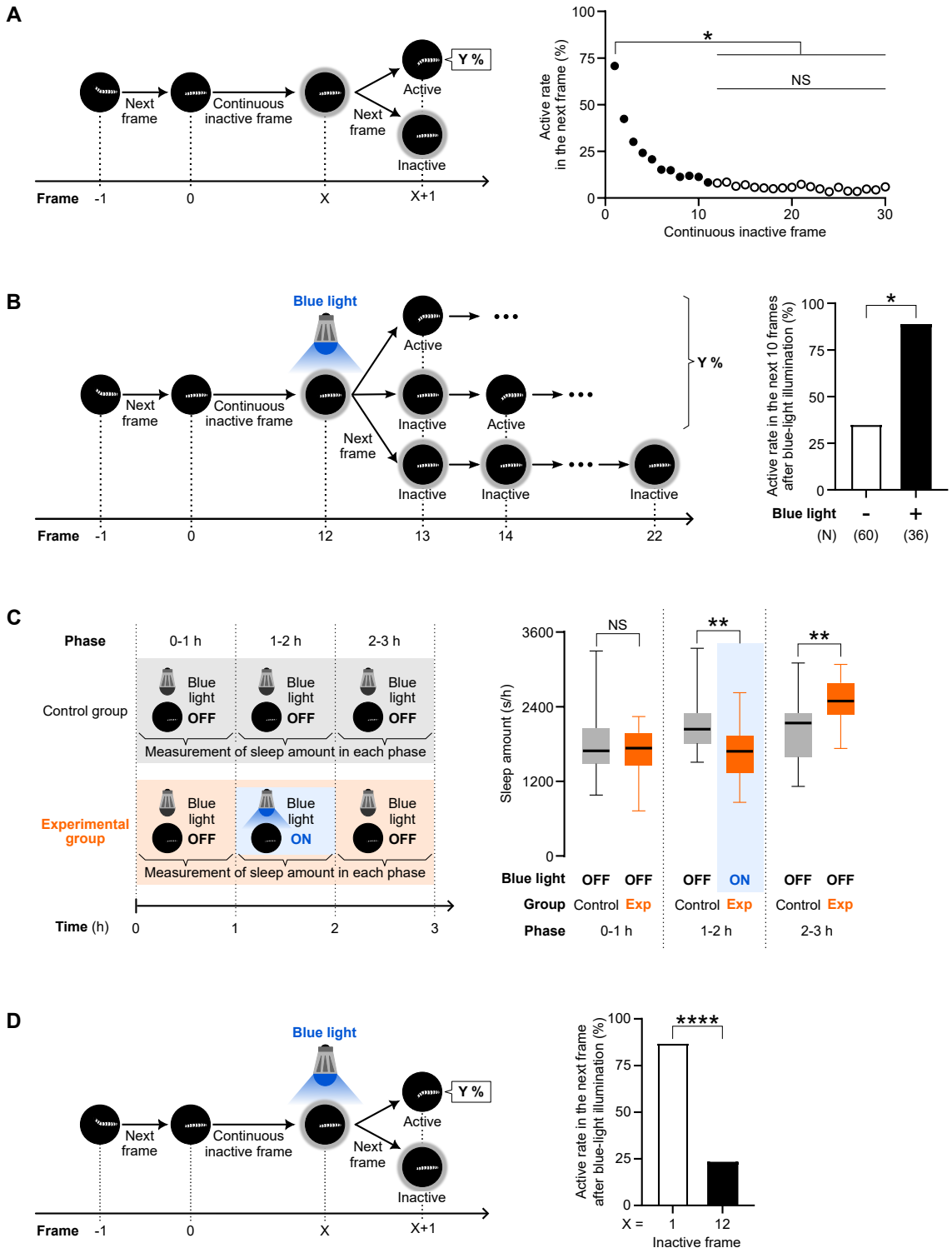

Figure 1—figure supplement 2. Larval "sleep state" in this study is consistent with behavioral criteria for sleep

(A) Relationship between "inactive" state duration and spontaneous arousal probability. Sustained quiescence for ≥ 12 frames (open circles) significantly reduced arousal

probability compared to 1-frame inactivity. * $p < 0.05$, NS: $p \geq 0.05$ (chi-squared test). (B) The percentage of larvae that showed a response within the next 10 frames after high-intensity blue light. The number of events analyzed was 36 and 60 with and without blue light irradiation, respectively. * $p < 0.05$ (Fisher's exact test). (C) Sleep amounts before, during, and after blue light irradiation. The number of larvae tested was 21 and 21 for the control and experimental groups, respectively. ** $p < 0.01$, NS: $p \geq 0.05$ (Mann–Whitney U-test with Bonferroni correction). (D) Percentage of larvae that showed a response in the next 1 or 12 frames after blue light stimulation. Number of events analyzed: 1960 or 111 for 1- or 12-frame continuous inactivity prior to blue light illumination, respectively. **** $p < 0.0001$ (chi-squared test).

Figure 1—figure supplement 3

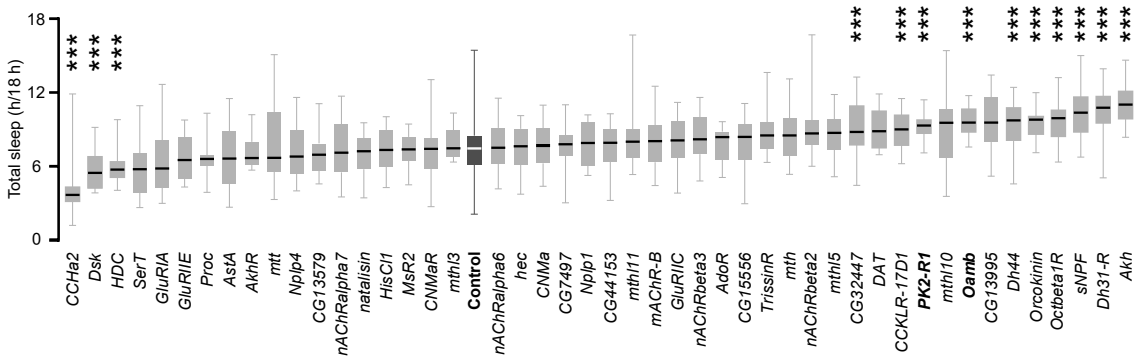

Figure 1—figure supplement 3. CRISPR-knock-out screen for genes that regulate larval sleep.

Total sleep amounts in CRISPR-knock-out mutants were measured for 18 h from the beginning of the second instar. The data for Control, *PK2-R1,* and *Oamb* mutants are identical to those shown in Figure 1. Box plots are generated so that the center line indicates the median, the box limits indicate the upper and lower quartiles, and the whiskers indicate the minimum-to-maximum range. *** $p < 0.005$ (Kruskal–Wallis one-way ANOVA and post hoc Mann–Whitney U-test with Bonferroni correction). Number of larvae tested: 475 for the control and 10–52 for each mutant.

Figure 1—figure supplement 4

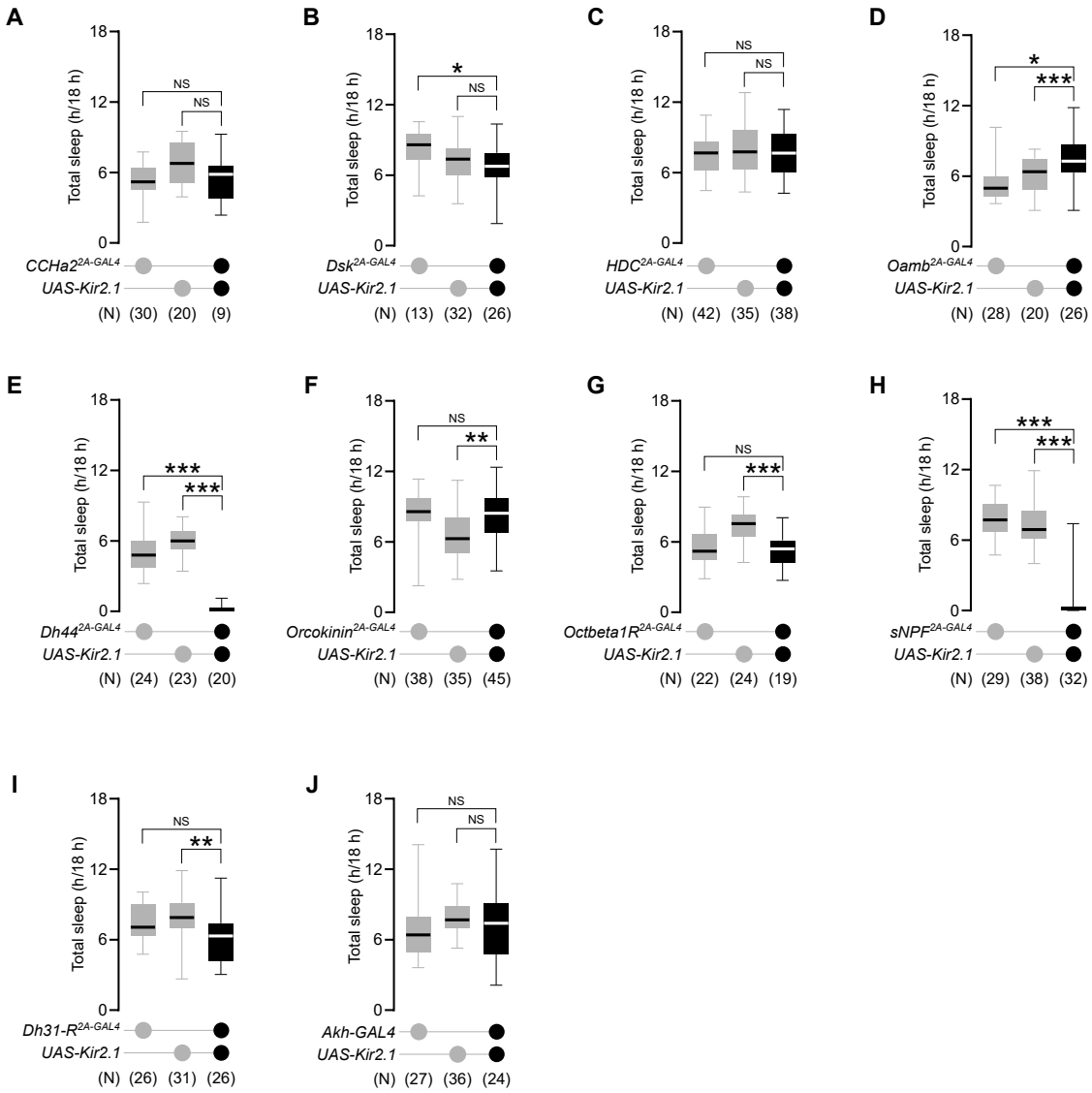

Figure 1—figure supplement 4. Effects of neuronal manipulation on larval sleep Sleep amounts in larvae in which distinct neuronal populations were silenced. Kir2.1 expression was driven by each enhancer-GAL4 for "hit" genes identified in the CRISPR-knock-out screen. 'N' indicates the number of biologically independent animals used for each group. Box plots are generated so that the center line indicates the median, the box limits indicate the upper and lower quartiles, and the whiskers indicate the minimum-to-maximum range. *** $p < 0.001$, ** $p < 0.01$, * $p < 0.05$, NS: ≥ 0.05 (Mann–Whitney U-test with Bonferroni correction).

Figure 2

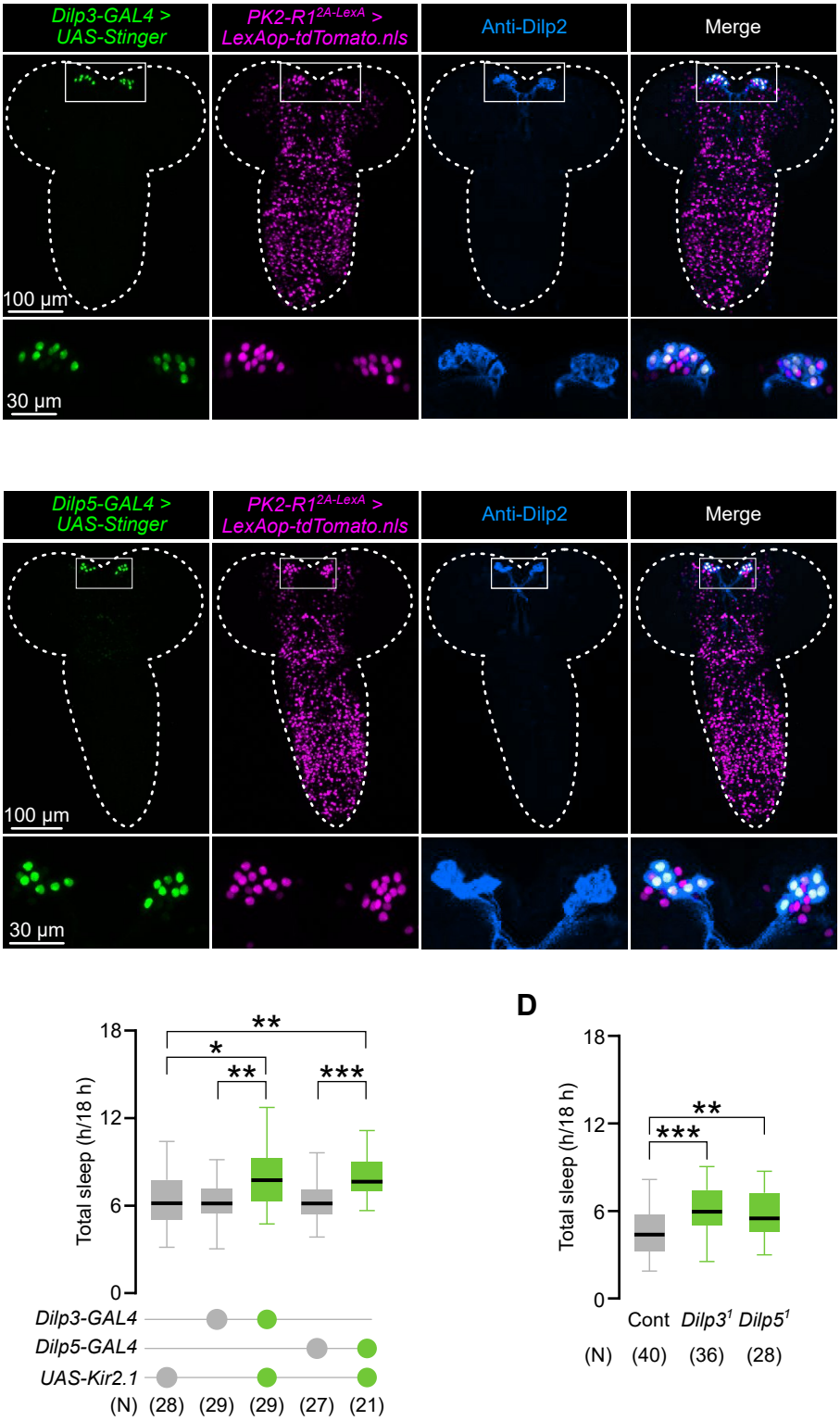

Figure 2. IPCs and Dilps negatively regulate larval sleep

988 (A) Triple labeling of *PK2-R1* neurons expressing nuclear-localized RFP (magenta),
989 *Dilp3* neurons expressing nuclear-localized GFP (green), and anti-Dilp2 positive cells
990 (blue). Top panels show signals in the larval brain and the VNC. The bottom panels
991 show magnified images of the white-squared area in the top panels, where the cell
992 bodies of the IPCs are located. Note that all IPCs labeled by *Dilp3-GAL4* are also
993 labeled by $PK2\text{-}R1^{2A\text{-}LexA}$. Similar results were obtained across five independent
994 samples. (B) Triple labeling of *PK2-R1* neurons expressing nuclear-localized RFP
995 (magenta), *Dilp5* neurons expressing nuclear-localized GFP (green), and anti-Dilp2
996 positive cells (blue). Similar results were obtained across five independent samples. (C)
997 Effect of IPCs silencing on larval sleep. In this and the following panels, 'N' indicates
998 the number of biologically independent animals used for each group. Box plots are
999 generated so that the center line indicates the median, the box limits indicate the upper
1000 and lower quartiles, and the whiskers indicate the minimum-to-maximum range. *** p
1001 < 0.001, ** $p < 0.01$, * $p < 0.05$ (Mann–Whitney U-test with Bonferroni correction).
1002 (D) Sleep amounts in *Dilp3* or *Dilp5* null mutant larvae. *** $p < 0.001$, ** $p < 0.01$
1003 (Mann–Whitney U-test with Bonferroni correction).

1004

1005

Figure 2—figure supplement 1

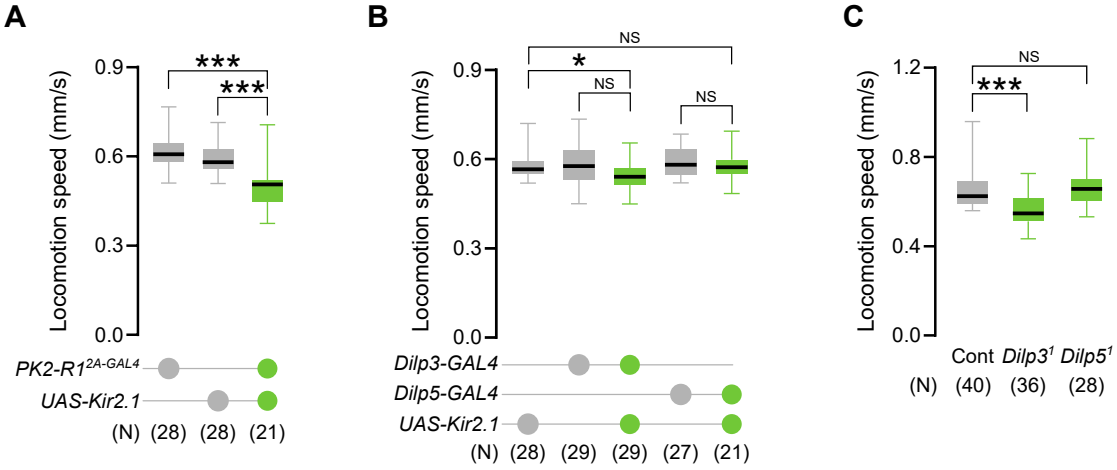

Figure 2—figure supplement 1. Locomotion speeds are not consistently affected by genetical manipulations of *PK2-R1*, IPCs, or *Dilps*

(A–B) Effects of silencing *PK2-R1* neurons (A) and IPCs (B) on larval locomotion speed. (C) Larval locomotion speed in null mutants of *Dilp3* or *Dilp5*. The average locomotion speed during the wake periods was measured from the data presented in Figures 1B, 2C, and 2D. In this and the following panels, 'N' indicates the number of biologically independent animals used for each group. Box plots are generated so that the center line indicates the median, the box limits indicate the upper and lower quartiles, and the whiskers indicate the minimum-to-maximum range. *** $p < 0.0001$, * $p < 0.05$, NS: $p \geq 0.05$ (Mann–Whitney U-test with Bonferroni correction).

Figure 3

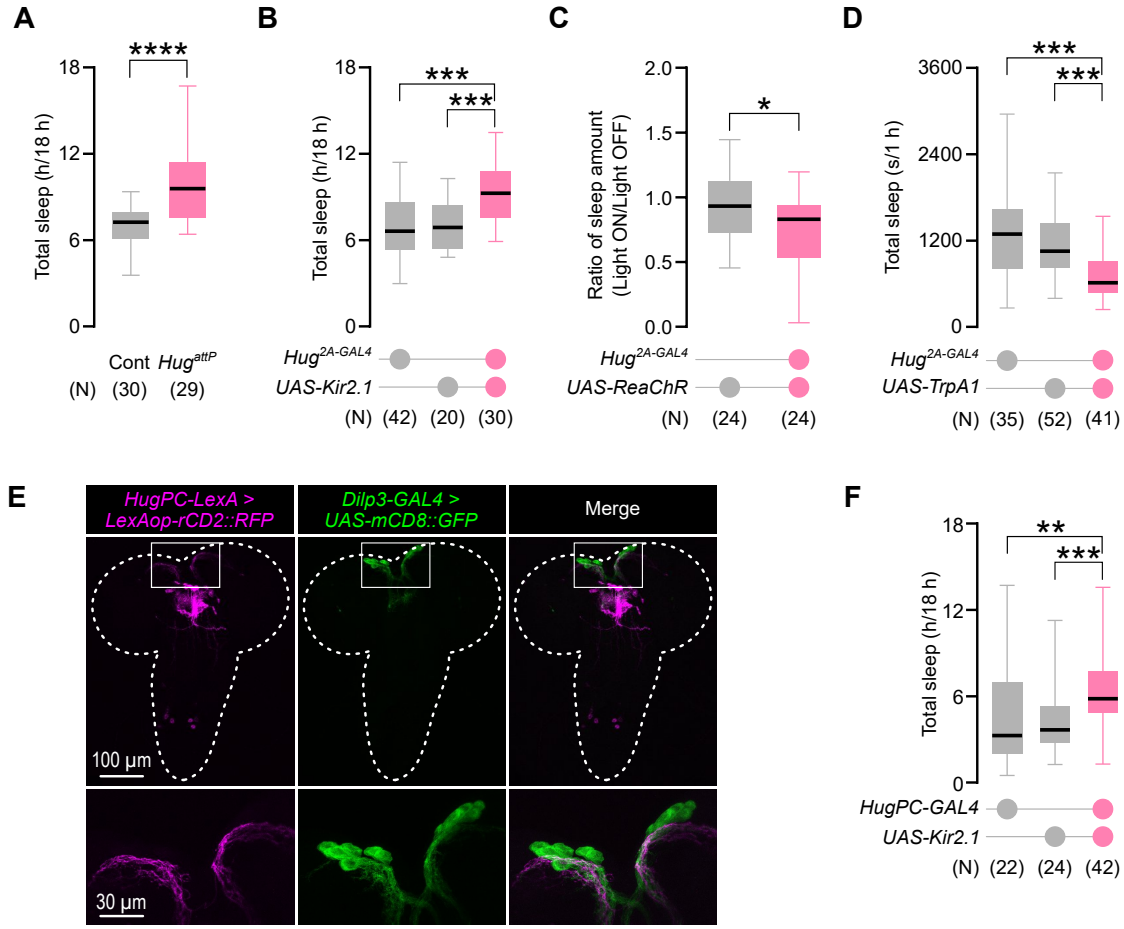

Figure 3. *Hug* neurons negatively regulate larval sleep

(A) Sleep amounts in *Hug* CRISPR-knock-out mutant larvae. In this and the following panels, 'N' indicates the number of biologically independent animals used for each group. Box plots are generated so that the center line indicates the median, the box limits indicate the upper and lower quartiles, and the whiskers indicate the minimum-to-maximum range. **** $p < 0.0001$ (Mann–Whitney U-test). (B) Effect of silencing *Hug* neurons on larval sleep amount. *** $p < 0.001$ (Mann–Whitney U-test with Bonferroni correction). (C) Larval sleep changes induced by optogenetic activation of *Hug* neurons. For each genotype, sleep duration in the 1-h light-ON period was normalized to that in the 1-h light-OFF phase. * $p < 0.05$ (Mann–Whitney U-test). (D) Larval sleep during thermogenetic activation of *Hug* neurons. *** $p < 0.001$ (Mann–Whitney U-test with Bonferroni correction). (E) Images of HugPC neurons and IPCs labeled by rCD2::RFP (magenta) and mCD8::GFP (green), respectively. The bottom panels show magnified images of the white-squared region in the top panels, in which HugPC neurons project their axons close to the cell bodies of the IPCs. While the top panels are z-stacks of 122

1034 image slices (1 μm interval) covering the entire brain, the bottom panels are projections
1035 of 60 slices around the cell bodies of IPCs. Similar results were obtained across five
1036 independent samples. (F) Effect of silencing HugPC neurons on larval sleep. *** $p <$
1037 0.001, ** $p < 0.01$ (Mann–Whitney U-test with Bonferroni correction).

1038

Figure 3—figure supplement 1

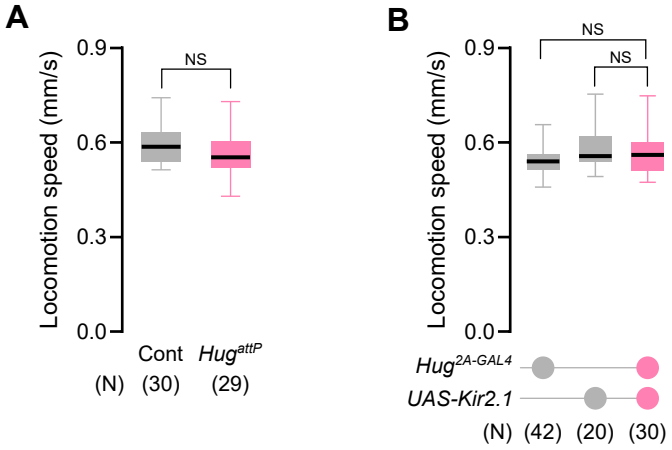

Figure 3—figure supplement 1. Neither *Hug* knock-out mutation nor *Hug* neuron silencing significantly affects larval locomotion speed

(A) Average locomotion speed of *Hug* knock-out mutants during waking periods. The data presented in Figures 3A and 3B were reanalyzed. In this and the following panels, 'N' indicates the number of biologically independent animals used for each group. Box plots are generated so that the center line indicates the median, the box limits indicate the upper and lower quartiles, and the whiskers indicate the minimum-to-maximum range. NS: $p \geq 0.05$ (Mann–Whitney U-test). (B) Locomotion speed of larvae in which *Hug* neurons were silenced. NS: $p \geq 0.05$ (Mann–Whitney U-test with Bonferroni correction).

Figure 3—figure supplement 2

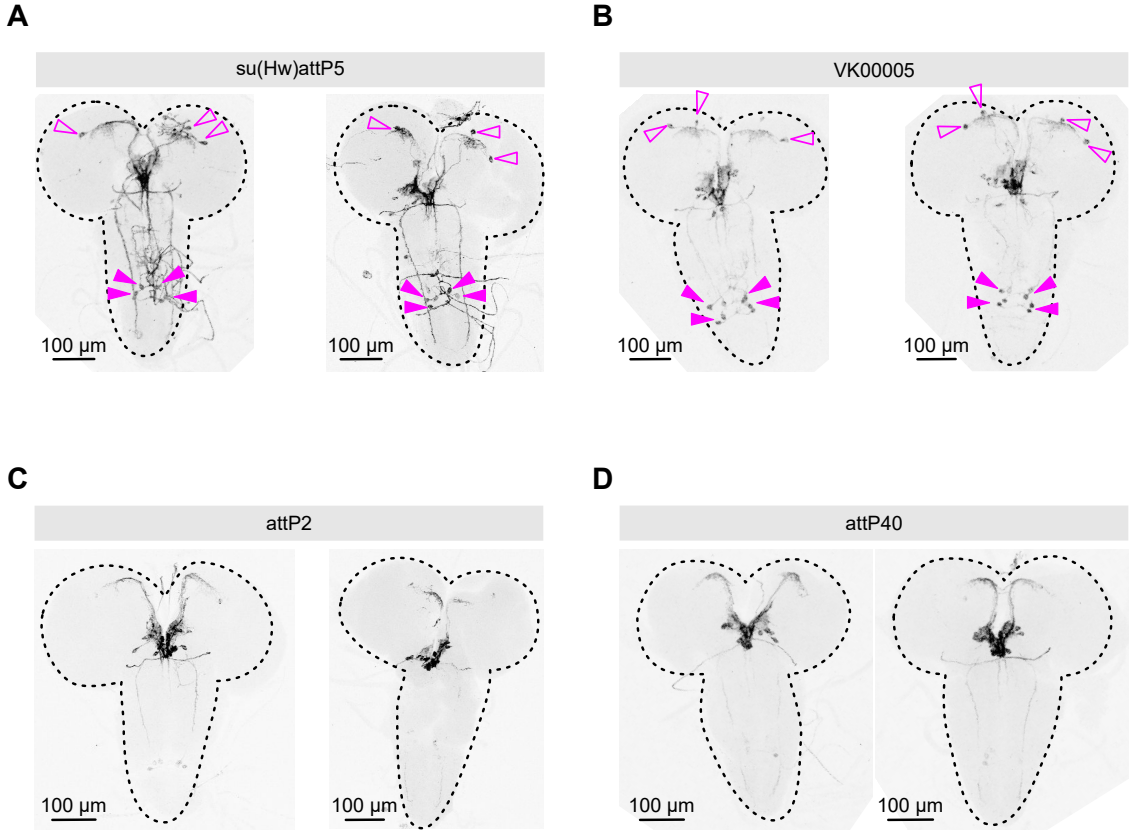

Figure 3—figure supplement 2. Generation of *HugPC-LexA* transgenic lines
(A–D) Labeling patterns of four *HugPC-LexA* strains in larval CNS visualized by rCD2::RFP. These transgenic lines were generated by injecting the identical plasmid into the following landing sites, respectively: su(Hw)attP5, VK00005, attP2, and attP40. Arrowheads indicate cell bodies of non-HugPC neurons. Filled and unfilled arrowheads indicate cell bodies within the VNC and near the protocerebrum, respectively.

Figure 4

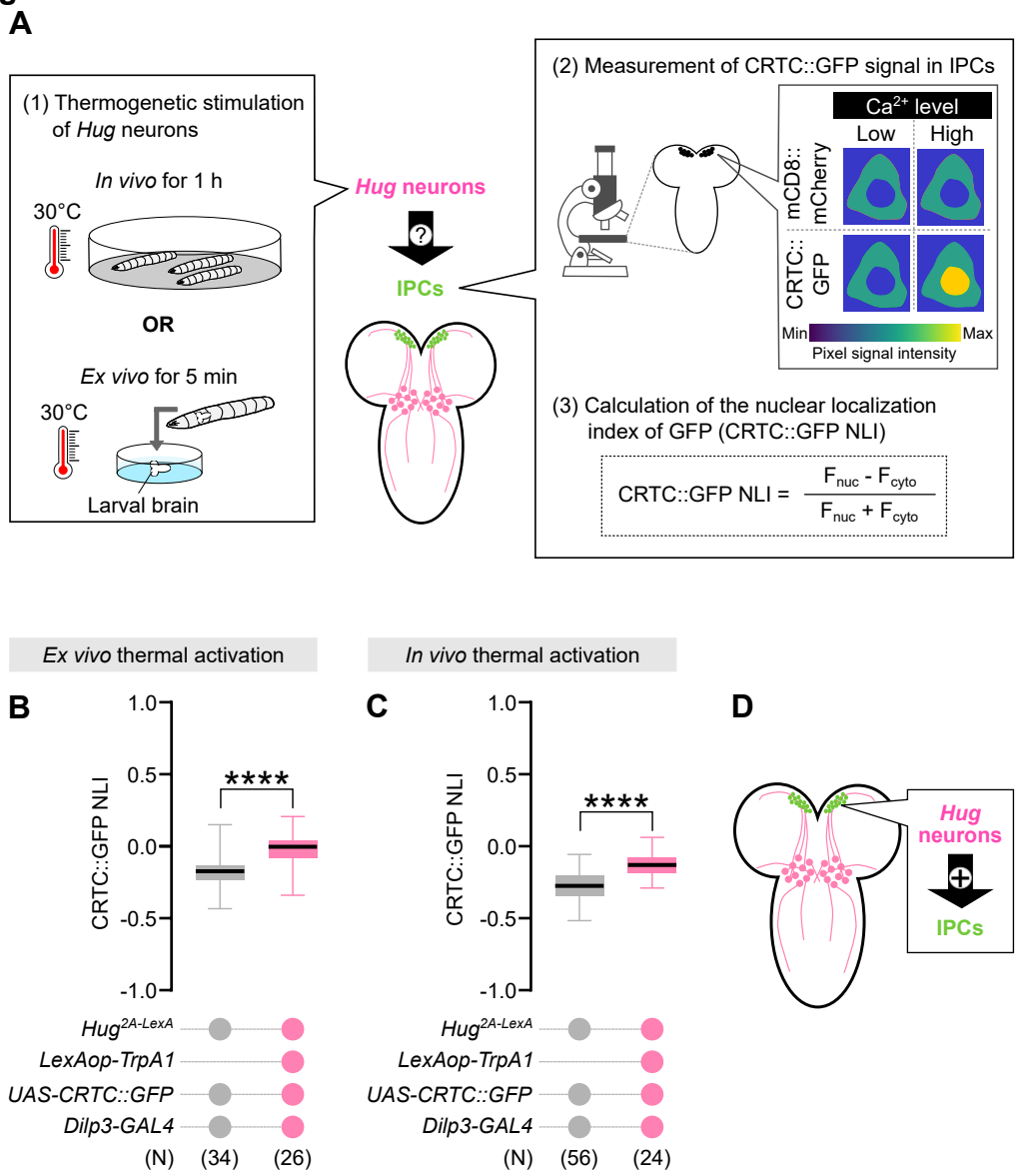

Figure 4. Activation of *Hug* neurons triggers Ca^{2+} responses in larval IPCs
(A) Schematic flow of assessing intracellular Ca^{2+} levels in IPCs while performing the thermogenetic activation of *Hug* neurons. (B–C) The level of nuclear-localized CRTC::GFP signal, calculated as NLI (see the Methods section for a detailed explanation of NLI), in IPCs during *Hug* neurons stimulation *ex vivo* (B) or *in vivo* (C). In these panels, 'N' indicates the number of cells used for each group. Box plots are generated so that the center line indicates the median, the box limits indicate the upper and lower quartiles, and the whiskers indicate the minimum-to-maximum range. **** $p < 0.0001$ (Mann–Whitney U-test). (D) The proposed neuronal connection that regulates larval sleep.

Figure 5

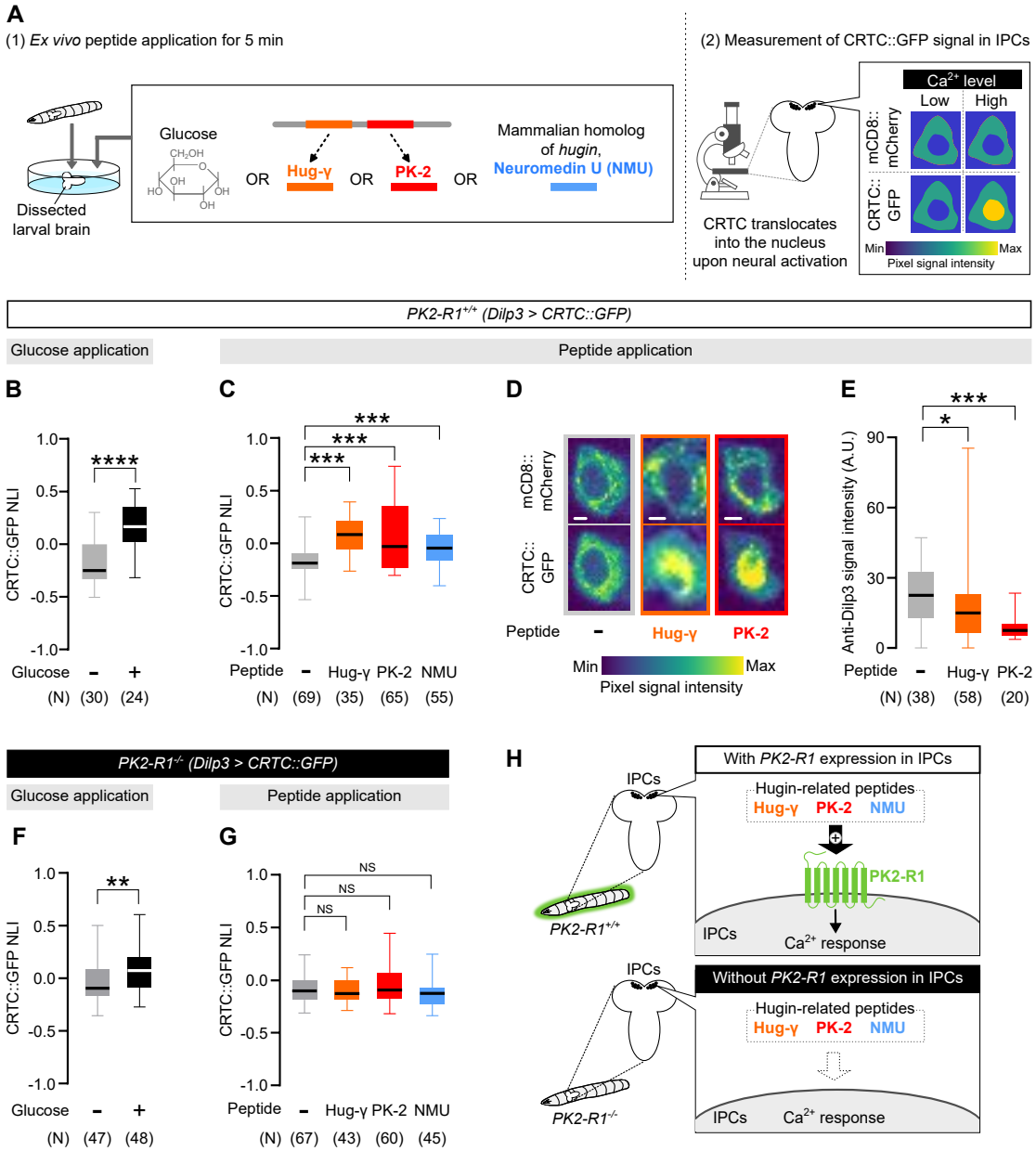

Figure 5. Hug peptides induce Ca^{2+} responses in larval IPCs via PK2-R1

(A) Schematic flow of assessing intracellular Ca^{2+} levels in IPCs and bath application of peptides. (B–C) Ca^{2+} responses in IPCs to *ex vivo* bath application of either glucose (B) or Hug peptides (C). In this and the following panels, 'N' indicates the number of cells used for each group. Box plots are generated so that the center line indicates the median, the box limits indicate the upper and lower quartiles, and the whiskers indicate the minimum-to-maximum range. **** $p < 0.0001$, *** $p < 0.001$ (Mann–Whitney U-test with Bonferroni correction). (D) Representative images of larval IPCs after peptide application. Scale bars, 2 μm. (E) Anti-Dilp3 signal intensity measured within the

1082 cytosolic areas of IPCs. *** $p < 0.001$, * $p < 0.05$ (Mann–Whitney U-test with Bonferroni
1083 correction). (F–G) Ca^{2+} responses in IPCs of *PK2-R1* knock-out mutants, measured
1084 following either glucose (F) or Hug peptide application (G). ** $p < 0.01$, NS: $p \geq 0.05$
1085 (Mann–Whitney U-test with Bonferroni correction). (H) A model where Hug peptides,
1086 but not glucose, activate IPCs via the PK2-R1 receptor.
1087
1088

Figure 5—figure supplement 1

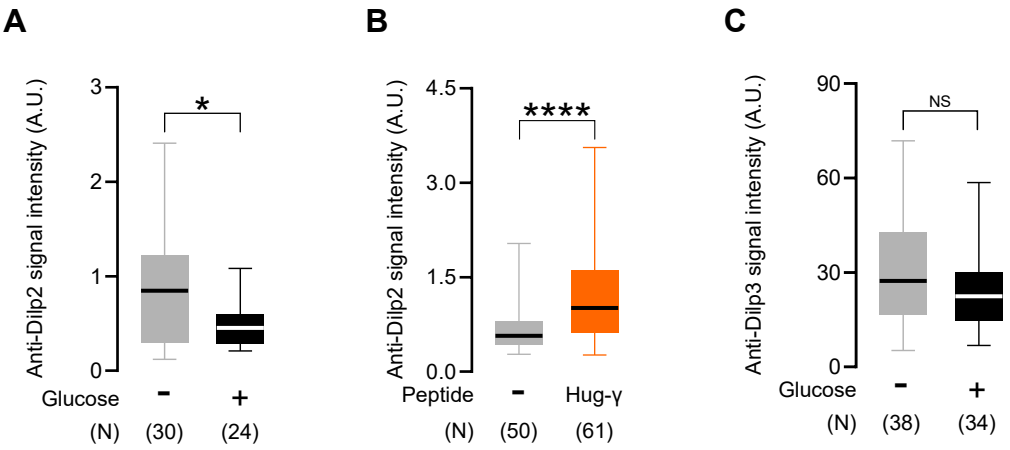

Figure 5—figure supplement 1. D-glucose but not Hug peptide cause Dilp2 reduction in IPCs

(A–B) Anti-Dilp2 signal intensity measured in IPCs after glucose (A) or Hug-γ application (B). In this and the following panels, 'N' indicates the number of cells used for each group. Box plots are generated so that center line indicates median, box limits indicate upper and lower quartiles, and whiskers indicate the minimum-to-maximum range. **** $p < 0.0001$, * $p < 0.05$ (Mann–Whitney U-test). (C) Anti-Dilp3 signal intensity measured within the cytosolic areas of IPCs. NS: ≥ 0.05 (Mann–Whitney U-test).

Figure 6

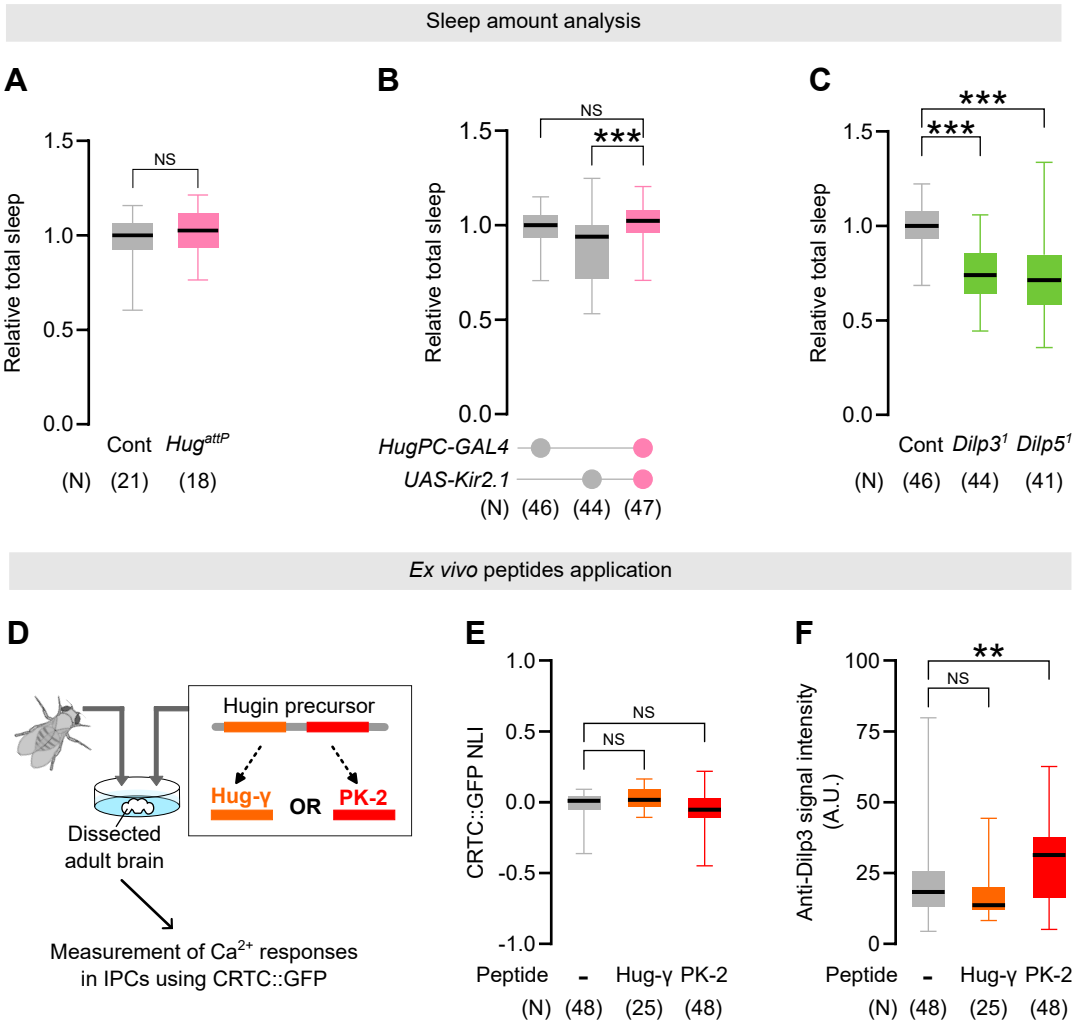

Figure 6. Distinct impacts of Hugin/PK2-R1 axis on wake/sleep control in larvae and adults

(A) Total sleep amounts in *Hug* knock-out mutant adults. NS: $p \geq 0.05$ (Mann–Whitney U-test). In these and the following panels, 'N' indicates the number of biologically independent animals used for each group. Box plots are generated so that the center line indicates the median, the box limits indicate the upper and lower quartiles, and the whiskers indicate the minimum-to-maximum range. NS: $p \geq 0.05$ (Mann–Whitney U-test). (B) Sleep amounts of adults in which HugPC neurons were silenced. *** $p < 0.001$, NS: $p \geq 0.05$ (Mann–Whitney U-test with Bonferroni correction). (C) Sleep amounts in *Dilp3* or *Dilp5* null mutant adults. *** $p < 0.001$ (Mann–Whitney U-test with Bonferroni correction). (D) Schematic flow of peptide application experiments using adult brains. (E–F) Ca^{2+} responses (E) and anti-Dilp3 signal intensity (F) in adult

IPCs after Hug peptide application. ** $p < 0.01$, NS: $p \geq 0.05$ (Mann–Whitney U-test with Bonferroni correction).

Figure 6—figure supplement 1

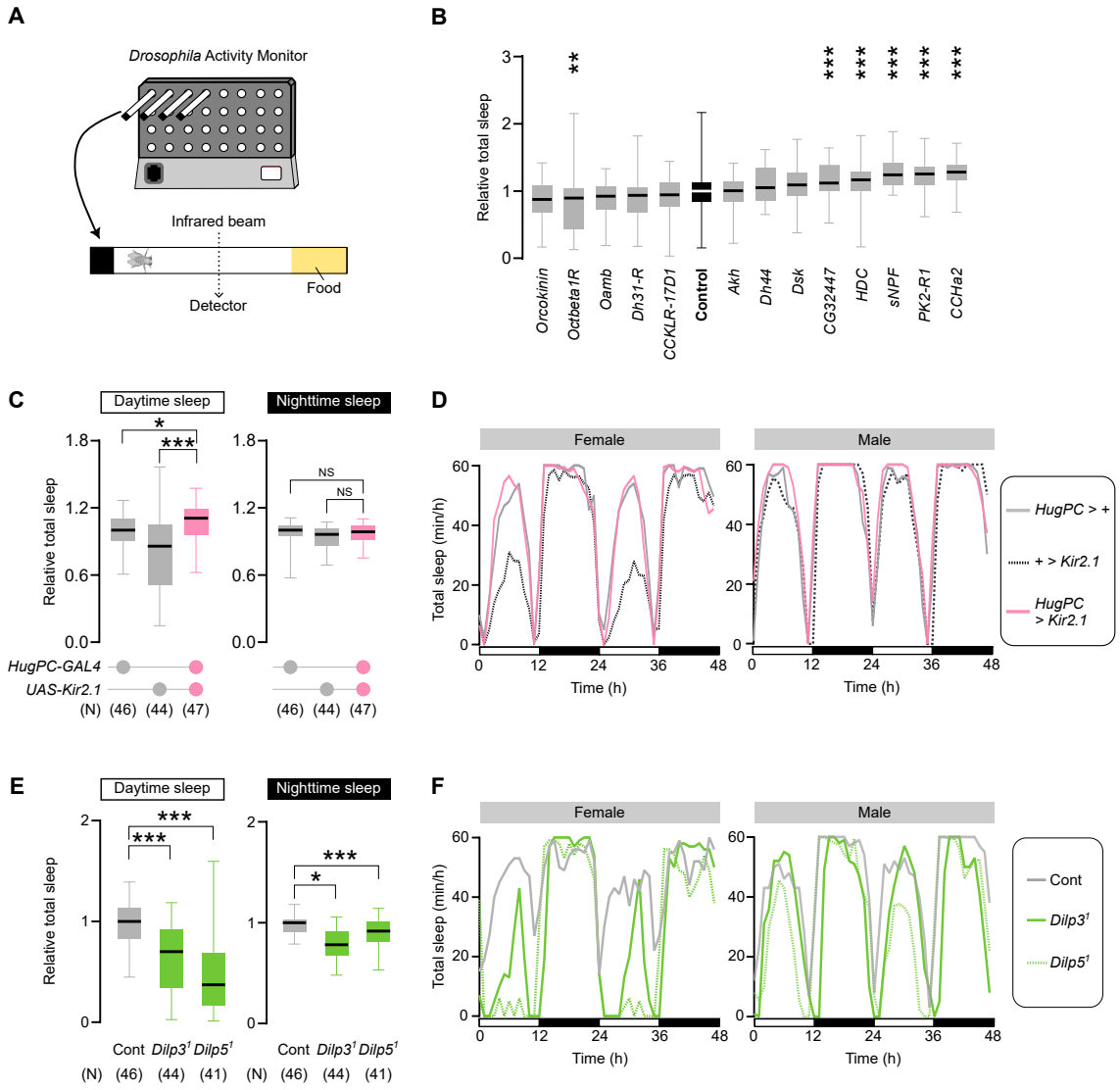

Figure 6—figure supplement 1. Sleep patterns of adult flies following manipulations of Hugin and insulin pathways

(A) Experimental setup for monitoring adult sleep using the *Drosophila* Activity Monitor (DAM). (B) Sleep duration in adult CRISPR-knock-out mutants. These mutants showed significant changes in the sleep amounts in larvae (Figure 1—figure supplement 3). In panels B, C, and E, sleep amounts were calculated as the ratio relative to the median sleep amount of the control group. Box plots are generated so that the center line indicates the median, the box limits indicate the upper and lower quartiles, and the whiskers indicate the minimum-to-maximum range. *** $p < 0.001$, ** $p < 0.01$ (Kruskal–Wallis one-way ANOVA and post hoc Mann–Whitney U-test with Bonferroni

correction). (C, E) Sleep amounts relative to the median value of the control group. Data presented in Figures 6B and 6C were reanalyzed. *** $p < 0.001$, * $p < 0.05$, NS: $p \geq 0.05$ (Mann–Whitney U-test with Bonferroni correction). (D, F) Temporal sleep patterns over two consecutive days.

Figure 6—figure supplement 2

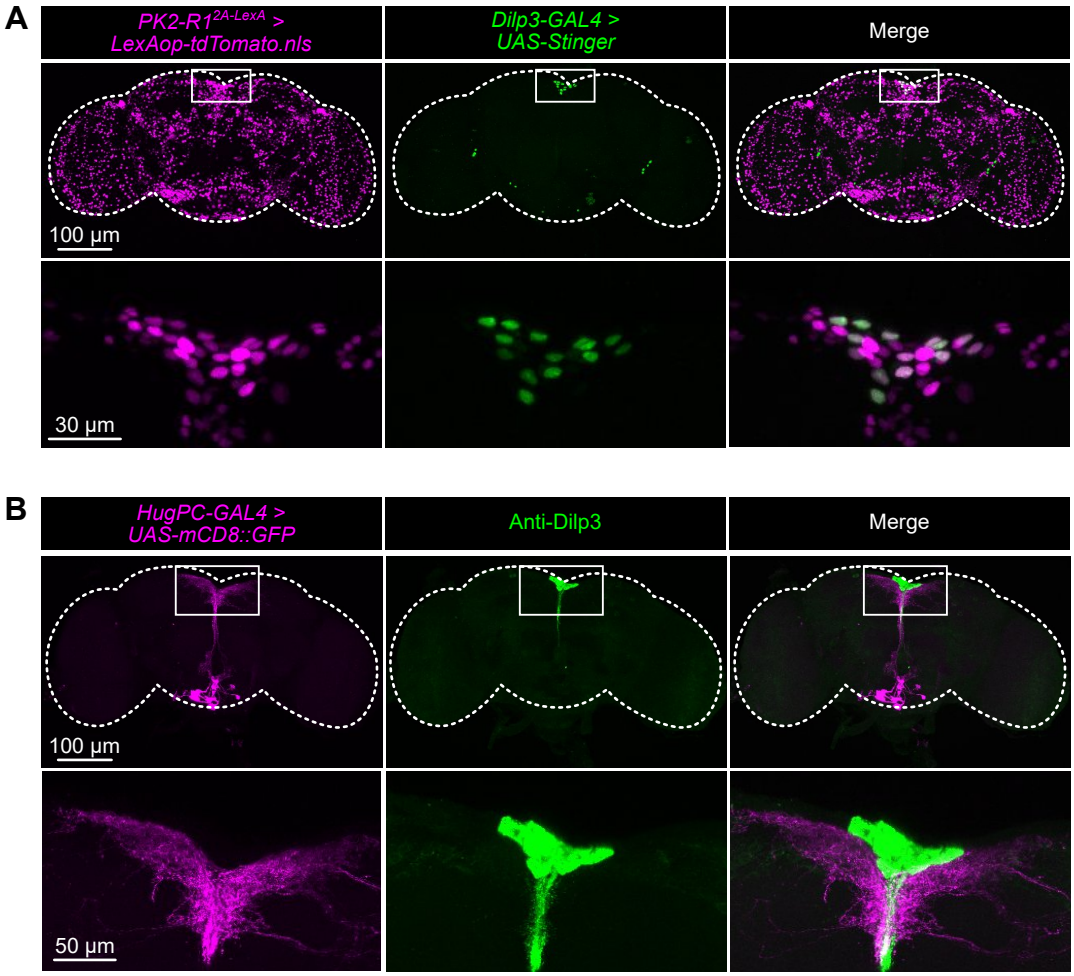

Figure 6—figure supplement 2. Morphology of *PK2-R1* neurons, HugPC neurons, and IPCs in the adult brain

(A) Dual labeling of *PK2-R1* neurons and IPCs expressing nuclear-localized RFP (stinger; magenta) and GFP (stinger; green), respectively. The top panels show signals in the entire adult brain. The bottom panels show magnified images of the white-squared area in each corresponding top panel, where the cell bodies of IPCs are located. Similar results were obtained across five independent samples. (B) Visualization of HugPC neurons and IPCs labeled by mCD8::GFP (magenta) and the anti-Dilp3 antibody (green), respectively. Similar results were obtained across four independent samples.

Figure 7

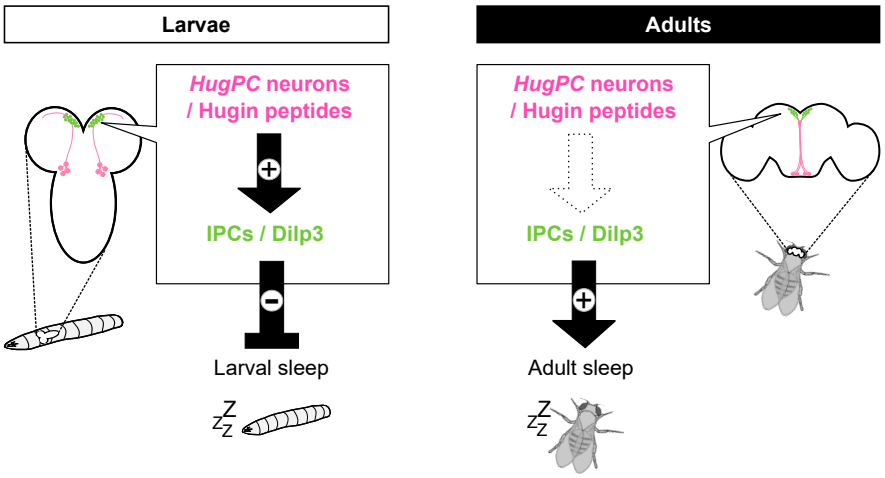

1150

1151 **Figure 7. A schematic model of the Hugin/PK2-R1/Dilps axis in larval and adult**

1152 **sleep regulation**

1153